High-Performance n-Channel Carbonyl-Functionalized Quaterthiophene Semiconductors: Thin-Film Transistor Response and Majority Carrier Type Inversion via Simple Chemical Protection/Deprotection

Myung-Han Yoon, Sara A. DiBenedetto, Matthew T. Russell, Antonio Facchetti,* and Tobin J. Marks*

Department of Chemistry and the Materials Research Center, Northwestern University, 2145 Sheridan Road, Evanston, Illinois 60208

Received May 7, 2007

The generalizable synthesis, comparative molecular physicochemical properties, film microstructures/morphologies, and field-effect transistor (FET) response characteristics of a series of six carbonyl-derivatized quaterthiophenes is described. These compounds are as follows: 5, 5‴-diheptanoyl-2,2′:5′,2″:5″,2‴-quaterthiophene (**1**), spiro[4H-cyclopenta[2,1-b:3,4-b′]dithiophene-4,2′-[1,3] dioxolane], 2,6-bis-(5-hexyl carbonylthien-2-yl) (**2**), 2,7-[bis-(5-hexylcarbonylthien-2-yl)]-4H-cyclopenta[2,1-b:3,4-b′]-dithiophen-4-one (**3**), 5, 5‴-diperfluorohexylcarbonyl-2,2′:5′,2″:5″,2‴-quaterthiophene (**4**), spiro[4H-cyclopenta[2,1-b:3,4-b′]dithiophene-4,2′- [1,3]dioxolane], 2,6-bis-(5-perfluorohexylcarbonylthien-2-yl) (**5**), and 2,7-[bis-(5-perfluorohexylcarbonylthien-2-yl)]-4H-cyclopenta[2,1-b:3,4-b′]-dithiophen-4-one (**6**). Optical and electrochemical data demonstrate that terminal/central carbonyl-functionalization of the quaterthiophene core strongly lowers both HOMO and LUMO energies. However, the extent of LUMO lowering is far greater than HOMO lowering with the outcome that the carbonyl-containing quaterthiophenes exhibit lower energy gaps than the corresponding parent systems. This greater LUMO stabilization is confirmed by electrochemical data and fully explained by DFT computations. OTFT measurements show that all of the six semiconductors are FET-active, and very large n-type (up to 0.32 cm^2/Vs), p-type (up to 0.04 cm^2/Vs), and ambipolar (up to 0.12 cm^2/Vs for electrons, 0.008 cm^2/Vs for holes) mobilites are observed depending on the exact quaterthiophene backbone architecture. A simple Schottky injection barrier model in combination with molecular packing and thin-film molecular orientation/morphology characteristics of **1**−**6** explain the observed OFET performance trends. Finally, FET majority charge carrier inversion (p-type → n-type) via *in situ* chemical deprotection of the central carbonyl functionality (**5** and **6**) is demonstrated for the first time and is attractive for sensor functions as well as for patterning complementary circuits. The latter is demonstrated in a simple contact patterning process.

Introduction

During the past decade, the field known as "organic" or "plastic electronics", in which the active (semi)conducting materials as well as dielectrics and other passive components are ideally composed of organic small molecules or polymers, has developed dramatically, involving many academic and industrial research groups.[1] Some of these efforts have resulted in commercialized products, principally in the areas of light emission and sensors. Despite this success and the potential for growth that this field offers, organic-based devices currently occupy a very small portion of the global electronics market. However, it is projected that organic electronic materials may be a viable alternative to silicon in many electronic and electro-optical applications where high speed is not a central issue or where conventional inorganic materials cannot compete. Such products might include electronic paper/flexible displays, printed radio frequency-powered electronics, and electronic sensors.[2]

One of the key elements in such unconventional electronics is the organic thin-film transistor (OTFT), and in terms of critical materials components, the OTFT is composed of a conductor, insulator/dielectric, and one or more semiconductors. Inferior semiconducting performance as well as poor

* Corresponding author e-mail: a-facchetti@northwestern.edu (A.F.) and t-marks@northwestern.edu (T.J.M.).

(1) (a) Singh, Th. B.; Sariciftci, N. S. *Annu. Rev. Mater. Res.* **2006**, *36*, 199. (b) Sirringhaus, H. *Adv. Mater.* **2005**, *17*, 2411. (c) Newman, C. R.; Frisbie, C. D.; da Silva Filho, D. A.; Bredas, J.-L.; Ewbank, P. C.; Mann, K. R. *Chem. Mater.* **2004**, *16*, 4436. (d) Horowitz, G. *J. Mater. Res.* **2004**, *19*, 1946. (e) Dimitrakopoulos, C. D.; Malenfant, P. R. L. *Adv. Mater.* **2002**, *14*, 99. (f) Dodabalapur, A. *Nature* **2005**, *434*, 151. (g) Barbarella, G.; Melucci, M.; Sotgiu, G. *Adv. Mater.* **2005**, *17*, 1581. (h) Tulevski, G. S.; Miao, Q.; Afzali, A.; Graham, T. O.; Kagan, C. R.; Nuckolls, C. *J. Am. Chem. Soc.* **2006**, *128*, 1788. (i) Rogers, J. A.; Bao, Z.; Katz, H. E.; Dodabalapur A. In *Thin-Film Transistors*; Kagan, C. R., Andry, P., Eds.; Marcel Dekker, Inc.: New York, 2003; pp 377−425. (j) *Printed Organic and Molecular Electronics*; Gamota, D. R., Brazis, P., Kalyanasundaram, X., Zhang, J., Eds.; Kluwer Academic Publishers: New York, 2004. (k) *Handbook of Oligo- and Polythiophenes*; Fichou, D., Ed.; Wiley-VCH: Weinheim, Germany, 1999. (l) *Handbook of Conductive Polymers*; Skotheim, T. A., Elsenbaumer, R. L., Reynolds, J. R., Eds.; Marcel Dekker: New York, 1998; pp 325−326. (m) Hotta, S. In *Handbook of Organic Conductive Molecules and Polymers*; Nalwa, H. S., Ed.; John Wiley & Sons: Chichester, 1997; Vol. 2, Chapter 8. (n) *Polythiophenes - Electrically Conductive Polymers;* Schopf, G., Kossmehl, G., Eds.; Springer: Berlin, 1997.

10.1021/cm071230g CCC: $37.00
Published on Web 09/01/2007

understanding of organic semiconductor charge trapping, especially in electron-transporting (n-type) materials, has been a significant impediment to applications using these organic-based devices. For this reason, OTFT research has principally focused on improving organic semiconductor performance.[3] To date, most organic semiconductors have been hole-transporting (p-type) materials, and there have been intense efforts to demonstrate performance parameters that rival/surpass those of amorphous silicon. Acenes[4] such as pentacene for vapor-phase semiconductor deposition, and solution-deposited polythiophenes[5] such as poly(3-alkyl thiophenes) for solution-phase semiconductor deposition, have been central in these efforts. Although it is now recognized that n-type semiconductors are crucial for the realization of complementary integrated circuits to reduce power consumption and enhance device speed, until recently there were only very few potentially applicable materials known in this category.[6]

Understanding the interplay between molecular/crystal structure and OTFT device characteristics has been fundamental to developing efficient p-type semiconductors, which can also be solution-processable. For example, it has been found that judicious functionalization of the aromatic π-conjugated cores with various substituents results in greatly improved p-type semiconductor performance.[3] In the search for high-performance n-type semiconductors, distinctly different synthetic approaches have been pursued, such as known n-type cores (e.g., nathphalene diimide, perylene diimide, C_{60}) to enhance processibility and device stability in air or "flipping" the majority carrier type of 'electron-rich' p-type cores (e.g., oligothiophenes, CuPc, acenes) by introducing strong electron-withdrawing functionalities such as F, fluorocarbons, and CN.[6] Regarding the latter, we previously demonstrated the use of fluorocarbon substituents to create efficient n-type oligothiophene semiconductors with good solubility and processability.[7−9]

(2) (a) Noguchi, Y.; Sekitani, T.; Someya, T. *Appl. Phys. Lett.* **2006**, *89*, 253507/1. (b) Chabinyc, M.; Loo, Y.-L. *J. Macromol. Sci., Pol. Rev.* **2006**, *46*, 1−5. (c) Locklin, J.; Roberts, M.; Mannsfeld, S.; Bao, Z. *J. Macromol. Sci., Pol. Rev.* **2006**, *46*, *79*. (d) Lee, K. J.; Motala, M. J.; Meitl, M. A.; Childs, W. R.; Menard, E.; Shim, A. K.; Rogers, J. A.; Nuzzo, R. G. *Adv. Mater.* **2005**, *17*, 2332. (e) Sele, C. W.; von Werne, T.; Friend, R. H.; Sirringhaus, H. *Adv. Mater.* **2005**, *17*, 997. (f) Park, J.; Shim, S.-O.; Lee, H. H. *Appl. Phys. Lett.* **2005**, *86*, 073505. (g) Chabinyc, M. L.; Salleo, A.; Wu, Y.; Liu, P.; Ong, B. S.; Heeney, M.; McCulloch, I. *J. Am. Chem. Soc.* **2004**, *126*, 13928. (h) Chabinyc, M. L.; Salleo, A. *Chem. Mater.* **2004**, *16*, 4509. (i) Ling, M. M.; Bao, Z. *Chem. Mater.* **2004**, *16*, 4824. (j) Lefenfeld, M.; Blanchet, G.; Rogers, J. *Adv. Mater.* **2003**, *15*, 1188.

(3) (a) Yamamoto, T.; Takimiya, K. *J. Am. Chem. Soc.* **2007**, *129*, 2224. (b) Ponomarenko, S. A.; Kirchmeyer, S.; Elschner, A.; Alpatova, N. M.; Halik, M.; Klauk, H.; Zschieschang, U.; Schmid, G. *Chem. Mater.* **2006**, *18*, 579. (c) Zhang, H.; Wang, Y.; Shao, K.; Liu, Y.; Chen, S.; Qiu, W.; Sun, X.; Qi, T.; Ma, Y; Yu, G.; Su, Z.; Zhu, D. *Chem. Commun.* **2006**, 755. (d) Ofuji, M.; Lovinger, A. J.; Kloc, C.; Siegrist, T.; Maliakal, A. J.; Katz, H. E. *Chem. Mater.* **2005**, *17*, 5748. (e) Wu, Y.; Ong, B. S. *J. Am. Chem. Soc.* **2005**, *127*, 3266. (f) Murphy, A. R.; Liu, J.; Luscombe, C.; Kavulak, D.; Frechet, J. M. J.; Kline, R. J.; McGehee, M. D. *Chem. Mater.* **2005**, *17*, 4892. (g) Locklin, J.; Li, D.; Mannsfeld, S. C. B.; Borkent, E.-J.; Meng, H.; Advincula, R.; Bao, Z. *Chem. Mater.* **2005**, *17*, 3366. (h) Payne, M. M.; Parkin, S. R.; Anthony, J. E. *J. Am. Chem. Soc.* **2005**, *127*, 8028. (i) Payne, M. M.; Parkin, S. R.; Anthony, J. E.; Kuo, C.-C.; Jackson, T. N. *J. Am. Chem. Soc.* **2005**, *127*, 4986. (j) Videlot-Ackermann, C.; Ackermann, J.; Ackermann, J.; Brisset, H.; Kawamura, K.; Yoshimoto, N.; Raynal, P.; El Kassmi, A.; Fages, F. *J. Am. Chem. Soc.* **2005**, *127*, 16346. (k) Sakamoto, Y.; Suzuki, T.; Kobayashi, M.; Gao, Y.; Fukai, Y.; Inoue, Y.; Sato, F.; Tokito, S. *J. Am. Chem. Soc.* **2004**, *126*, 8838. (l) Kunugi, Y.; Takimiya, K.; Toyoshima, Y.; Yamashita, K.; Aso, Y.; Otsubo, T. *J. Mater. Chem.* **2004**, *14*, 1367. (m) Mohapatra, S.; Holmes, B. T.; Newman, C. R.; Prendergast, C. F.; Frisbie, C. D.; Ward, M. D. *Adv. Funct. Mater.* **2004**, *14*, 605. (n) Yanagi, H.; Araki, Y.; Ohara, T.; Hotta, S.; Ichikawa, M.; Taniguchi, Y. *Adv. Funct. Mater.* **2003**, *13*, 767. (o) Casado, J.; Ruiz Delgado, M. C.; Shirota, Y.; Hernandez, V.; Lopez Navarrete, J. T. *J. Phys. Chem. B* **2003**, *107*, 2637. (p) Ichikawa, M.; Yanagi, H.; Shimizu, Y.; Hotta, S.; Suganuma, N.; Koyama, T.; Taniguchi, Y. *Adv. Mater.* **2002**, *14*, 1272. (q) Apperloo, J. J.; Groenendaal, L. B.; Verheyen, H.; Jayakannan, M.; Janssen, R. A. J.; Dkhissi, A.; Beljonne, D.; Lazzaroni, R.; Bredas, J.-L. *Chemistry* **2002**, *8*, 2384. (r) Moreno Castro, C.; Ruiz Delgado, M. C.; Hernandez, V.; Hotta, S.; Casado, J.; Lopez Navarrete, J. T. *J. Phys. Chem. B* **2002**, *116*, 10419. (s) Lee, S. A.; Yoshida, Y.; Fukuyama, M.; Hotta, S. *Synth. Met.* **1999**, *106*, 39.

(4) (a) Anthony, J. E. *Chem. Rev.* **2006**, *106*, 5028. (b) Schmidt, R.; Goettling, S.; Leusser, D.; Stalke, D.; Krause, A.-M.; Wuerthner, F. *J. Mater. Chem.* **2006**, *16*, 3708. (c) Abthagir, P. S.; Ha, Y.-G.; You, E.-A.; Jeong, S.-H.; Seo, H.-S.; Choi, J.-H. *J. Phys. Chem. B* **2005**, *109*, 23918. (d) Sun, Y.; Liu, Y.; Zhu, D. *J. Mater. Chem.* **2005**, *15*, 53. (e) Moon, H.; Zeis, R.; Borkent, E.-J.; Besnard, C.; Lovinger, A. J.;Siegrist, T.; Kloc, Ch.; Bao, Z. *J. Am. Chem. Soc.* **2004**, *126*, 15322. (f) Kelley, T. W.; Baude, P. F.; Gerlach, C.; Ender, D. E.; Muyres, D.; Haase, M. A.; Vogel, D. E.; Theiss, S. D. *Chem. Mater.* **2004**, *16*, 4413. (g) Ling, M. M.; Bao, Z. *Chem. Mater.* **2004**, *16*, 4824. (h) Jurchescu, O. D.; Baas, J.; Palstra, T. T. M. *Appl. Phys. Lett.* **2004**, *84*, 3061. (i) Brinkmann, M.; Graff, S.; Straupe, C.; Wittmann, J.-C.; Chaumont, C.; Nuesch, F.; Aziz, A.; Schaer, M.; Zuppiroli, L. *J. Phys. Chem. B* **2003**, *107*, 10531. (j) Shtei, M.; Mapel, J.; Benziger, J. B.; Forrest, S. R. *Appl. Phys. Lett.* **2002**, *81*, 268. (k) Klauk, H.; Jackson, T. N. *Solid State Technol.* **2000**, *43*, 63. (l) Lin, Y.-Y.; Gundlach, D. J.; Nelson, S. F.; Jackson, T. N. *IEEE Trans. Electron Devices Lett.* **1997**, *44*, 1325.

(5) (a) Kumar, P.; Chand, S.; Dwivedi, S.; Kamalasanan, M. N. *Appl. Phys. Lett.* **2007**, *90*, 023501/1. (b) Wagner, V.; Wobkenberg, P.; Hoppe, A.; Seekamp, J. *Appl. Phys. Lett.* **2006**, *89*, 243515/1. (c) Heeney, M.; Bailey, C.; Genevicius, K.; Shkunov, M.; Sparrowe, D.; Tierney, S.; McCulloch, I. *J. Am. Chem. Soc.* **2005**, *127*, 1078. (d) Ong, B. S.; Wu, Y. L.; Liu, P.; Gardner, S. *J. Am. Chem. Soc.* **2004**, *126*, 3378. (e) Rost, H.; Ficker, J.; Alonso, J. S.; Leenders, L.; McCulloch, I. *Synth. Met.* **2004**, *145*, 83. (f) Chang, J. F.; Sun, B. Q.; Breib, D. W.; Nielsen, M. M.; Solling, T. I.; Giles, M.; McCulloch, I.; Sirringhaus, H. *Chem. Mater.* **2004**, *16*, 4772. (g) Wang, G. M.; Swensen, J.; Moses, D.; Heeger, A. J. *J. Appl. Phys.* **2003**, *93*, 6137. (h) Ficker, J.; Ullmann, A.; Fix, W.; Rost, H.; Clemens, W. *J. Appl. Phys.* **2003**, *94*, 2638. (i) Sirringhaus, H.; Tessler, N.; Friend, R. H. *Science* **1998**, *280*, 1741. (j) Bao, Z.; Dodabalapur, A. J.; Lovinger, A. J. *Appl. Phys. Lett.* **1996**, *69*, 4108.

(6) (a) Sun, Y.; Rohde, D.; Liu, Y.; Wan, L.; Wang, Y.; Wu, W.; Di, C.; Yu, G.; Zhu, D. *J. Mater. Chem.* **2006**, *16*, 4499. (b) Chikamatsu, M.; Nagamatsu, S.; Yoshida, Y.; Saito, K.; Yase, K.; Kikuchi, K. *Appl. Phys. Lett.* **2005**, *87*, 203504/1. (c) Ando, S.; Nishida, J.; Tada, H.; Inoue, Y.; Tokito, S.; Yamashita, Y *J. Am. Chem. Soc.* **2005**, *127*, 5336. (d) Jones, B. A.; Ahrens, M. J.; Yoon, M.-H.; Facchetti, A.; Marks, T. J.; Wasielewski, M. R. *Angew. Chem., Int. Ed.* **2004**, *43*, 6363. (e) Sakamoto, Y.; Suzuki, T.; Kobayashi, M.; Gao, Y.; Fukai, Y.; Inoue, Y.; Sato, F.; Tokito, S. *J. Am. Chem. Soc.* **2004**, *126*, 8138. (f) Facchetti, A.; Mushrush, M.; Katz, H. E.; Marks, T. J. *Adv. Mater.* **2003**, *15*, 33. (g) Kobayashi, S.; Takenobu, T.; Mori, S.; Fujiwara, A.; Iwasa, Y. *Appl. Phys. Lett.* **2003**, *82*, 4581. (h) Pappenfus, T. M.; Chesterfield, R. J.; Frisbie, C. D.; Mann, K. R.; Casado, J.; Raff, J. D.; Miller, L. L. *J. Am. Chem. Soc.* **2002**, *124*, 4184. (i) Malenfant, P. R.; Dimitrakopoulos, C. D.; Gelorme, J. D.; Kosbar, L. L.; Graham, T. O. *Appl. Phys. Lett.* **2002**, *80*, 14. (j) Heidenhain, S. B.; Sakamoto, Y.; Suzuki, T.; Miura, A.; Fujikawa, H.; Mori, T.; Tokito, S.; Taga, Y. *J. Am. Chem. Soc.* **2000**, *122*, 10240. (k) Katz, H. E.; Lovinger, A. J.; Johnson, J.; Kloc, C.; Siegrist, T.; Li, W.; Lin, Y.-Y.; Dodabalapur, A. *Nature* **2000**, *404*, 478. (l) Facchetti, A.; Deng, Y.; Wang, A.; Koide, Y.; Sirringhaus, H.; Marks, T. J.; Friend, R. H. *Angew. Chem., Int. Ed.* **2000**, *39*, 4547. (m) Bao, Z.; Lovinger, A. J.; Brown, J. *J. Am. Chem. Soc.* **1998**, *120*, 207. (n) Haddon, R. C.; Perel, A. S.; Morris, R. C.; Palstra, T. T. M.; Hebard, A. F.; Fleming, R. M. *Appl. Phys. Lett.* **1995**, *67*, 121.

(7) (a) Facchetti, A.; Mushrush, M.; Yoon, M.-H.; Hutchison, G. R.; Ratner, M. A.; Marks, T. J. *J. Am. Chem. Soc.* **2004**, *126*, 13859. (b) Facchetti, A.; Yoon, M.-H.; Stern, C. L.; Hutchison, G. R.; Ratner, M. *J. Am. Chem. Soc.* **2004**, *126*, 13480. (c) Hutchison, G. R.; Ratner, M. A.; Marks, T. J. *J. Phys. Chem. B* **2005**, *109*, 3126, and references therein.

(8) Facchetti, A.; Yoon, M.-H.; Stern, C. L.; Katz, H. E.; Marks, T. J. *Angew. Chem., Int. Ed.* **2003**, *42*, 3900.

Chart 1. Oligothiophene Semiconductors

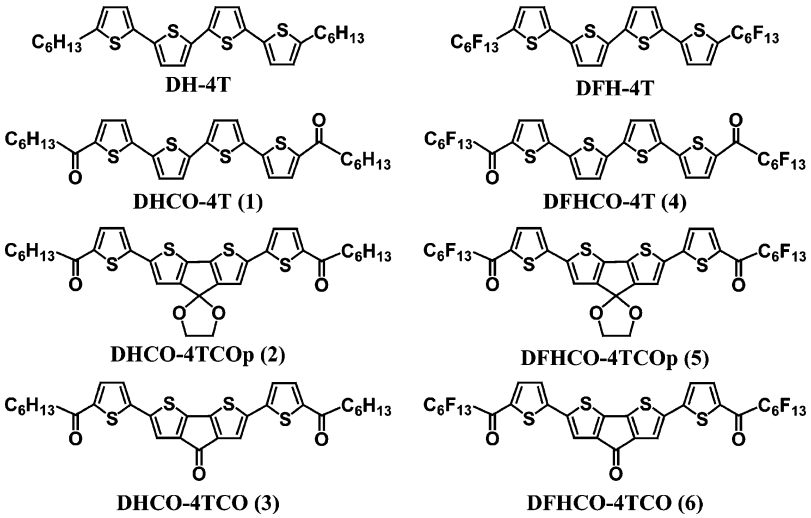

Following a similar approach for tuning oligothiophene properties via selected α,ω-substitution, the synthesis of three new acyl-/fluoroacyl-substituted quaterthiophenes with large n-type/ambipolar mobilites was reported in a preliminary communication.[10] In the present contribution, we now present a full discussion of our studies of acyl/fluoroacyl-derivatized oligothiophenes, aimed at better understanding the effects of this unique substituent on organic semiconductor molecular properties and on those of the corresponding thin films. The carbonyl functionalities investigated here include both long-chain acyl and perfluoroacyl groups installed at the oligothiophene α,ω positions as well as bridged dioxolane and carbonyl groups positioned at the center of the molecular core. To achieve this goal, the synthesis of expanded semiconductor series **1**−**6** (Chart 1) is reported along with detailed electronic and crystallographic structural characterization as well as characterization of the corresponding OTFT devices fabricated with these materials. We compare and contrast their properties with those of the carbonyl-free derivatives **DH-4T** and **DFH-4T** and parent quaterthiophene (α4T). In the present study, molecular characterization of **1**−**6** includes optical spectroscopy, thermal analysis (including the elucidation of liquid-crystalline phase formation), cyclic voltammetry, and single-crystal X-ray diffraction (XRD), while vapor-deposited thin-film microstructures and morphologies are investigated by wide-angle X-ray diffraction (WAXRD) and scanning electron microscopy (SEM). DFT electronic structure computations are performed to understand optical and electrochemical trends. Transistor devices are fabricated via both vapor phase and solution film growth techniques.

Through the thermal and single-crystal structural information it will be seen that C═O incorporation enhances mesophase formation tendencies and strongly alters molecular packing characteristics from the typical herringbone motif of α4T, **DH-4T**, and **DFH-4T** to slipped cofacial packing. Optical and electrochemical characterization demonstrates that terminal/central carbonyl-functionalization of the quaterthiophene core strongly enhances electron affinity and ionization potential. The magnitude of these effects will be seen to be far larger than observed previously for oligothiophene semiconductors used in OFETs. Furthermore, C═O functionalized molecules **1**−**6** exhibit a significant reduction of the optical/electrochemical HOMO−LUMO gap vs. the parent alkyl/perfluoroalkyl-substituted quaterthiophenes. This result is fully explained through DFT computations which reveal a unique property of C═O introduction in lowering LUMO energies substantially more than the HOMO energies. Importantly, all of these new semiconductors are OFET-active, and OFET performance characteristics reveal definitive correlations between majority charge carrier type, electrochemically derived MO energies, and charge carrier injection rates. Mobilities (n-type) as high as 0.34 cm^2/Vs with current ratios as high as $\sim 10^6$, and ambipolar charge transport are highlights observed for members of this new materials class. We also demonstrate that proper solution film growth strategies afford OFETs with performace metrics only slightly inferior to films fabricated by vapor-phase deposition, which is important for eventual large-scale OFET fabrication. In addition, we report the first demonstration of FET majority charge carrier inversion (p-type → n-type) via chemical protection/deprotection in the DFHCO-4TCOp → DFHCO-4TCO conversion. This chemically induced carrier conversion is readily patternable using a new PDMS stamping method to form p-n junctions (as demonstrated herein) and is attractive for sensors and complementary organic circuits.

Experimental Section

Materials. Acyl- and perfluoroacyl-derivatized quaterthiophenes **1**−**6** and intermediate products **7**−**10** and **12** were straightforwardly synthesized as shown in Scheme 1. The final products, semiconductors **1**−**6**, were purified by either gradient vacuum sublimation (1×10^{-4} Torr) or recrystallization (from hot xylene). The reagents 5,5′-bis(tri-n-butylstannyl)-2,2′-dithiophene[11] and compound **11**[12] were prepared according to published procedures. Other chemical reagents were purchased from Aldrich Chemical Co. unless

(9) Yoon, M.-H.; DiBenedetto, S.; Facchetti, A.; Marks, T. J. *J. Am. Chem. Soc.* **2005**, *127*, 1348.
(10) Letizia, J. A.; Facchetti, A.; Stern, C. L.; Ratner, M. A.; Marks, T. J. *J. Am. Chem. Soc.* **2005**, *127*, 13476.
(11) Wei, Y.; Yang, Y.; Yeh, J.-M. *Chem. Mater.* **1996**, *8*, 2659.

Scheme 1. Synthetic Routes to Semiconductors 1−6

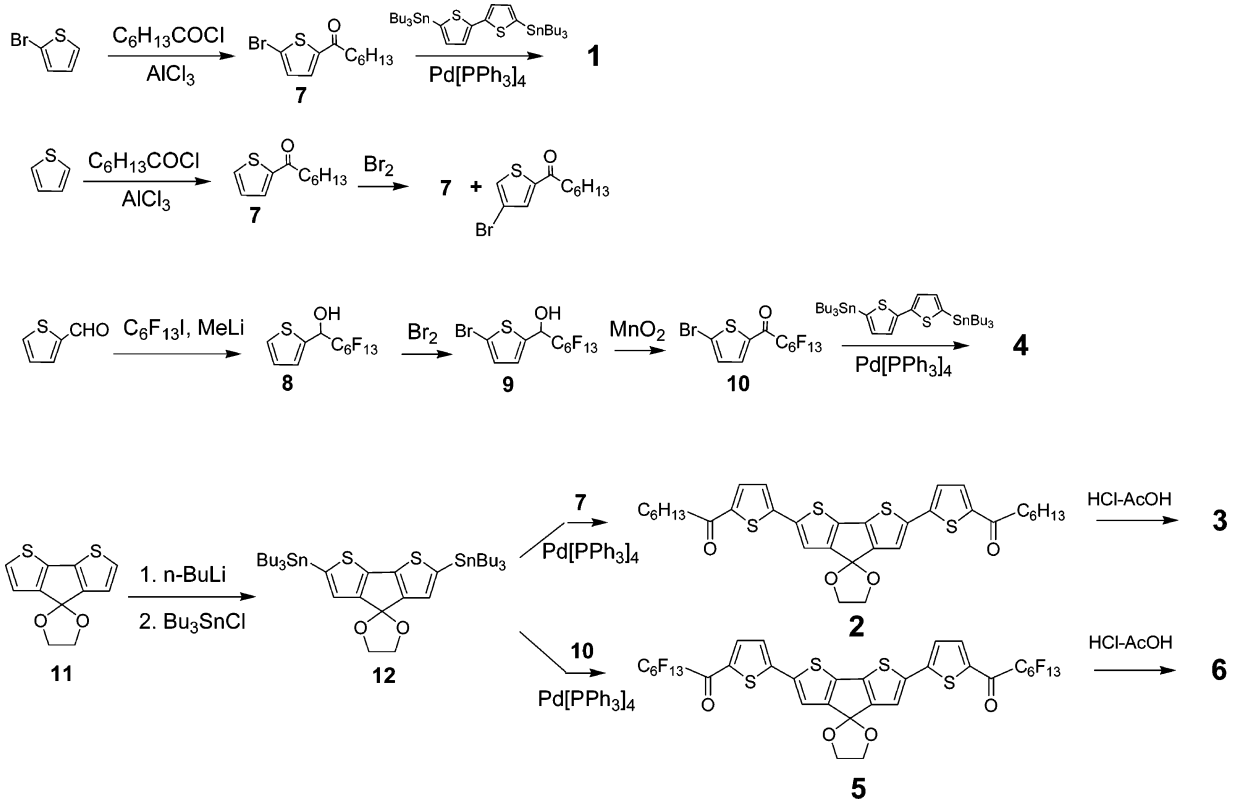

otherwise indicated. All new compounds were characterized by mass spectrometry, elemental analysis (Midwest Microlab), and ^{1}H and/or ^{19}F NMR (Varian Mercury 400). NMR data are not available for compounds **3** and **6** due to the poor solubility in common NMR solvents.

Synthesis of 5, 5‴-Diheptanoyl-2,2′:5′,2″:5″,2‴-quaterthiophene (DHCO-4T, 1). A mixture of compound **7** (0.64 g, 2.33 mmol), 5,5′-bis(tri-n-butylstannyl)-2,2′-dithiophene (0.744 g, 1.00 mmol), and tetrakis(triphenylphosphine)palladium(0) (0.070 g, 0.060 mmol) in dry DMF (5 mL) was deaerated three times with N_2. The reaction mixture was then stirred overnight at 100 °C during which time a precipitate formed. After having been cooled, the orange solid was collected by filtration and washed several times with hexane and then with MeOH. The orange solid was recrystallized from xylene and dried in a vacuum oven (120 °C) yielding a pure product (0.36 g, 65% yield): mp 290 °C; ^{1}H NMR (CD_2Cl_2): δ 7.60 (d, 2H, ^3J = 3.6 Hz), 7.25 (d, 2H, ^3J = 3.6 Hz), 7.19 (d, 2H, ^3J = 3.6 Hz), 7.16 (d, 2H, ^3J = 3.6 Hz), 2.85 (t, 4H, ^3J = 7.6 Hz), 1.72−1.70 (m, 4H), 1.36−1.31 (m, 12H), 0.88 (t, 4H, ^3J = 6.0 Hz). Anal. Calcd for $C_{30}H_{34}O_2S_4$: C 64.94, H 6.18. Found: C 64.80, H 6.21. MS (EI): *m/z* (%) 553.9 (100) [M^+].

Synthesis of Spiro[4H-cyclopenta[2,1-b:3,4-b′]dithiophene-4,2′-[1,3]dioxolane], 2,6-bis-(5-hexyl carbonylthien-2-yl) (DHCO-4TCOp, 2). A mixture of compound **7** (1.40 g, 4.92 mmol), compound **12** (2.00 g, 2.46 mmol), and $Pd[PPh_3]_4$ (0.193 g, 0.167 mmol) in dry DMF (20 mL) was stirred overnight at 100 °C. The red solution was allowed to cool slowly to room temperature and then filtered. The disubstituted product was collected as ruby-red, needle-shaped crystals and washed several times with hexane and then ether. The solid was recrystallized from xylene and dried in a vacuum oven (120 °C) to yield a pure compound (1.00 g, 63% yield): mp 180−181 °C; ^{1}H NMR (CD_2Cl_2): δ 7.59 (d, 2H, ^3J = 4.4 Hz), 7.192 (2H), 7.14 (d, 2H, ^3J = 4.4 Hz), 4.36 (4H), 2.86 (t, 4H, ^3J = 7.4 Hz), 1.72−1.77 (m, 4H), 1.37−1.33 (m, 12 H), 0.90 (t, 4H, ^3J = 6.4 Hz). Anal. Calcd for $C_{33}H_{36}O_4S_4$: C 63.43, H 5.81. Found: C 63.26, H 5.76. MS (EI, 70 eV) *m/z*: (M^+) calcd for $C_{33}H_{36}O_4S_4$:624.7; found: 624.1.

Synthesis of 2,7-[Bis-(5-hexylcarbonylthien-2-yl)]-4H-cyclopenta[2,1-b:3,4-b′]-dithiophen-4-one (DHCO-4TCO, 3). Compound **2** (0.33 g, 0.537 mmol) was refluxed in acetic acid. After addition of concentrated HCl (1.2 mL), a gray solid formed immediately. The mixture was stirred for an additional 5 min before it was quenched with H_2O (12 mL). The warm solution was then filtered to collect the gray solid, which was washed twice with acetone and chloroform. The solid was dried in a vacuum oven overnight and purified by gradient sublimation twice (0.21 g, 64% yield): mp 260−262 °C. Anal. Calcd for $C_{31}H_{32}O_3S_4$: C 64.10, H 5.55. Found: C 63.94, H 5.34. MS (EI, 70 eV) *m/z*: (M^+) calcd for $C_{31}H_{32}O_3S_4$: 580.6; found: 580.1.

Synthesis of 5, 5‴-Diperfluorohexylcarbonyl-2,2′:5′,2″:5″,2‴-quaterthiophene (DFHCO-4T, 4). A mixture of compound **10** (1.86 g, 3.66 mmol), 5,5′-bis(tri-b-butylstannyl)-2,2′-dithiophene (1.36 g, 1.83 mmol), and tetrakis(triphenylphosphine)palladium-(0) (0.13 g, 0.11 mmol) in dry DMF (10 mL) was deaerated three times with N_2. The reaction mixture was stirred overnight at 100 °C during which time a precipitate formed. After having been cooled, the dark red solid was collected by filtration and washed several times with hexane and then with MeOH. Further purification was achieved by gradient vacuum sublimation (1.22 g, 65% yield): mp 248 °C; ^{1}H NMR (CD_2Cl_2): δ 7.93 (2H), 7.39 (2H), 7.32 (2H), 7.27 (2H); ^{19}F NMR (CD_2Cl_2): δ −79.88 (6F), −113.42 (4F), −120.18 (8F), −121.62 (4F), −124.90 (4F). Anal. Calcd for $C_{30}H_8F_{26}O_2S_4$: C 35.24, H 0.79, F 48.30. Found: C 35.13, H 0.84, F 48.51. MS (EI): *m/z* (%) 1021.5 (100) [M^+].

Synthesis of Spiro[4H-cyclopenta[2,1-b:3,4-b′]dithiophene-4,2′-[1,3]dioxolane], 2,6-bis-(5-perfluorohexyl carbonylthien-2-yl) (DFHCO-4TCOp, 5). A mixture of compound **12** (2.00 g, 2.46 mmol), compound **10** (2.50 g, 4.91 mmol), and $Pd[PPh_3]_4$ (0.193 g, 0.167 mmol) in dry DMF (60 mL) was stirred at 90 °C for 6 h. After 15 min, a purple solid precipitated. Decantation of the red

supernatant left the disubstituted product as a dark green solid (2.18 g, 81% yield). The solid was washed with ether (3 × 20 mL) and hexane (3 × 10 mL), dried overnight in a vacuum oven, and purified by gradient sublimation: mp 218 °C; ^{1}H NMR ($CDCl_3$): δ 7.88 (2H), 7.32 (4H), 4.39 (4H); ^{19}F NMR (DMSO): δ 85.88 (6F), −119.69 (4H), −126.43 (8F), −127.85 (4F), −131.21 (4F); Anal. Calcd for $C_{33}H_{10}F_{26}O_4S_4$: C 36.27, H 0.92. Found: C 36.15, H 1.01. MS (EI, 70 eV) *m/z*: (M^+) calcd for $C_{33}H_{10}F_{26}S_4O_4$: 1092.4; found: 1092.2.

Synthesis of 2,7-[Bis-(5-perfluorohexylcarbonylthien-2-yl)]-4H-cyclopenta[2,1-b:3,4-b′]-dithiophen-4-one (DFHCO-4TCO, 6). Compound **5** (0.50 g, 0.46 mmol) was dissolved in 75 mL of acetic acid with refluxing. After addition of concentrated HCl (2 mL), the solution turned from purple to brown, and a dark green precipitate formed immediately. The reaction was next quenched with H_2O (20 mL). The supernatant solution was then decanted while warm, and the product was collected as a dark green solid (0.45 g). The solid was washed with acetone (2 × 10 mL) and chloroform (6 × 10 mL), dried overnight in a vacuum oven, and purified by gradient sublimation twice. The pure portion was collected and washed with boiling chloroform (20 mL). The red solution was decanted, leaving the product as a black solid. It was washed with chloroform and further purified by gradient sublimation (0.265 g, 60% yield): mp 297 °C. Anal. Calcd for $C_{31}H_6F_{26}O_3S_4$: C 35.51, H 0.58. Found: C 35.40, H 0.71. MS (EI, 70 eV) *m/z*: calcd (M^+) for $C_{31}H_6F_{26}S_4O_3$, 1048.0; found, 1048.0.

Synthesis of 2-Heptanoyl-5-bromothiophene (7). The reagents 2-bromothiophene (1.63 g, 10.0 mmol) and n-heptanoyl chloride (1.78 g, 12.0 mmol) were dissolved in dry benzene (15 mL), and $AlCl_3$ was added in portions with stirring over a period of 10 min. The resulting dark brown solution was next refluxed for 1 h and left to cool to room temperature. The reaction mixture was then quenched with 2 M HCl (15 mL) while carefully stirring. The organic layer was separated, washed with 2 M HCl, 2 M NaOH, and water, and passed through a silica column (width = 3 cm, length = 8 cm). The collected solution was dried over $MgSO_4$ and filtered, and the filtrate was concentrated *in vacuo* to yield the desired product as a colorless solid (2.40 g, 87% yield): ^{1}H NMR ($CDCl_3$): δ 7.44 (d, 1H, ^3J = 3.8 Hz), 7.10 (d, 1H, ^3J = 3.8 Hz), 2.81 (t, 2H, ^3J = 7.4 Hz), 1.74−1.68 (m, 2H), 1.38−1.23 (m, 6H), 0.89 (t, 3H, ^3J = 6.4 Hz); HRMS (EI, 70 eV) *m/z*: calcd (M^+) for $C_{11}H_{15}BrOS$: 274.00; found: 274.0016.

Synthesis of Perfluorohexyl-thien-2-yl-methanol (8). MeLi (1.6 M, 15.9 mL) was added dropwise to a solution of 5-thiophenyl aldehyde (2.80 g, 25.0 mmol) and perfluorohexyliode (11.73 g, 26.3 g) in dry Et_2O (70 mL) at −78 °C with stirring. The mixture was then stirred for an additional 40 min and quenched with 3 N HCl (70 mL). The organic layer was separated, washed with water twice, dried over $MgSO_4$, filtered, and concentrated *in vacuo*. Column chromatography of the residue on silica gel (hexane:ethyl acetate = 1:1) yielded **8** as a colorless solid (6.20 g, 57% yield): ^{1}H NMR ($CDCl_3$): δ 7.45 (d, 1H, ^3J = 4.5 Hz), 7.24 (d, 1H, ^3J = 3.0 Hz), 7.10−7.06 (dd, 1H, ^3J = 4.5, 3.8 Hz), 5.54−5.46 (m, 1H), 2.56 (d, 1H, ^3J = 5.7 Hz); HRMS (EI, 70 eV) *m/z*: calcd (M^+) for $C_{11}H_5F_{13}$-OS: 431.99; found: 431.9838.

Synthesis of Perfluorohexyl-(5-bromothien-2-yl)methanol (9). Bromine (0.698 g, 4.37 mmol) was added to a solution of **8** (1.80 g, 4.16 mmol) in CH_2Cl_2 (15 mL). After stirring overnight at room temperature, the mixture was neutralized with saturated aqueous $NaHCO_3$ solution and extracted with CH_2Cl_2 (3 × 20 mL). The organic layers were combined, dried over $MgSO_4$, filtered, and concentrated *in vacuo* to afford the product as a light brown solid (1.90 g, 89% yield). This material is sufficiently pure to use for the next synthetic step. ^{1}H NMR ($CDCl_3$): δ 7.02 (d, 1H, ^3J = 3.7 Hz), 6.97 (d, 1H, ^3J = 3.8 Hz), 5.46−5.38 (m, 1H), 2.64 (d, 1H, ^3J = 5.2 Hz); HRMS (EI, 70 eV) *m/z*: calcd (M^+) for $C_{11}H_4F_{13}$-BrOS: 509.90; found: 509.8945.

Synthesis of 2-Perfluorohexylcarbonyl-5-bromothiophene (10). A solution of compound **9** (1.90 g, 3.72 mmol) in CH_2Cl_2 (30 mL) and activated MnO_2 (5.0 g, 5.75 mmol) was stirred overnight. The mixture was then filtered through Celite. The filtrate was dried over $MgSO_4$ and filtered, and the solvent was evaporated in vacuum to afford the crude product (1.85 g, 98% yield). The mixture was purified by vacuum sublimation to afford a brown solid: mp 27 °C; ^{1}H NMR ($CDCl_3$): δ 7.74 (d, 1H, ^3J = 3.8 Hz), 7.23 (d, 1H, ^3J = 3.8 Hz); ^{19}F NMR ($CDCl_3$): δ −81.20 (3F), −115.20 (2F), −121.77 (4F), −123.18 (2F), −126.53 (2F). Anal. Calcd for $C_{11}H_2BrF_{13}OS$: C 25.95, H 0.40. Found: C 26.11, H 0.54. MS (EI, 70 eV) *m/z*: (M^+) calcd for $C_{11}H_2BrF_{13}OS$: 509.8; found: 509.8.

Synthesis of Spiro[4H-cyclopenta[2,1-b:3,4-b′]dithiophene-4,2′-[1,3]dioxolane], 2,6-bis(tri-n-butylstannyl) (12). Spiro[4H-cyclopenta[2,1-b:3,4-b′]dithiophene-4,2′-[1,3]dioxolane] (1.71 g, 7.35 mmol) was dissolved in dry THF (20 mL) under nitrogen and cooled to −78 °C. Two equivalents of *n*-BuLi were added dropwise (5.92 mL, 14.85 mmol), and the reaction mixture was stirred for 30 min. The solution was then allowed to warm to room temperature and stirred for an additional 1.5 h. The resulting thick brown suspension was cooled again to −78 °C, and tri-*n*-butyltin chloride (4.78 g, 14.7 mmol) was added. The solution was then stirred at room temperature for 4 h. The reaction was quenched with 100 mL of H_2O and extracted with hexane. The organic layer was washed with H_2O (6 × 50 mL) and dried over $MgSO_4$. After filtration, evaporation of the solvent left a brown oil (5.7 g, 95% yield): ^{1}H NMR ($CDCl_3$): δ 6.96 (s, 2H), 4.33 (s, 4H), 1.57 (m, 12H), 1.33 (m, 12H), 1.10 (m, 12H), 0.91 (t, 18H, ^3J = 6.8 Hz); HRMS (ACPI, CH_2Cl_2) *m/z*: ($(M+H)^+$) calcd for $C_{35}H_{60}S_2O_2Sn_2$: 814.4; found: 815.2.

Thermal Analysis, Optical Spectrometry, and Electrochemistry. Differential scanning calorimetry (DSC) and thermogravimetric analysis (TGA) measurements were performed on a TA DSC 2920 and Mettler-Toledo TGA instruments, respectively. UV−vis absorption spectra were recorded on a Varian Cary 5E spectrophotometer and photoluminescence spectra on a Photon Technology International QM-2 fluorescence spectrometer. Cyclic voltammograms of compounds **1**−**6** were measured in 0.1 M TBAPF solutions in THF with scan rates 100 mV/s using a Bioanalytical Systems Epsilon potentiostat equipped with C3 Cell Stand. The formal potentials ($E^{1/2}$) were extracted as the midpoints between the peak potentials of the forward and reverse scans with respect to a ferrocene reference (+0.54 V).

Single-Crystal Structure Determination. Single crystals of **DHCO-4TCOp** were grown from hot xylene solution. X-ray single-crystal diffraction measurements were performed on a Bruker CCD area detector instrument with graphite-monochromated Mo Kα (0.71073 Å) radiation. The data were collected at 153(2) K, and the structures were solved by direct methods and expanded using Fourier techniques. Crystallographic details are reported in the Supporting Information.

Device Fabrication and Thin-Film Characterization. Prime grade p-doped silicon wafers (100) with 300 nm of thermally grown oxide (Montco Inc.) were used as device substrates. They were rinsed with acetone and ethanol and cleaned in an oxygen plasma (20W, 5 min) before hexamethyldisilazane (HMDS) treatment. Trimethylsilyl functionalization of the p^+-Si/SiO_2 surface was carried out by exposing the silicon wafers to HMDS vapor at room temperature in a closed container under nitrogen overnight. All organic films were deposited by either vacuum evaporation (pres-

sures $\sim 2 \times 10^{-6}$ Torr) at a growth rate of 0.2−0.3 Å s^{-1} or by casting films from 1,2,4-trichlorobenzene solutions (0.5−0.8 mg/mL). For solution-cast films, the warm solutions were transferred onto SiO_2/p^+-Si substrates at elevated temperatures and allowed to evaporate slowly in a saturated solvent vapor environment. Then, all cast films were annealed in a vacuum oven (100 °C) overnight. Evaporated films were ∼50 nm thick (as determined by a calibrated *in situ* quartz crystal monitor), whereas solution-cast films were variable in thickness and generally thicker, on the order of 100 nm. For *in situ* film conversion, vapor-deposited/solution-cast films of **DFHCO-4TCOp** on p^+-Si/SiO_2 and glass were exposed to a saturated atmosphere of H_2O + HCl vapors, while the substrate temperature was maintained at 150 °C for 1−2 h. Then the substrates were placed in the vacuum oven (100 °C) for 3 h to remove adsorbed water, HCl, and deprotected ethylene glycol. For TFT device fabrication, top-contact electrodes (500 Å) were deposited by evaporating gold (pressure $\sim 3 \times 10^{-6}$ Torr) through a shadow mask with channel dimensions of 100 μm (L) × 5.0 mm (W). The capacitance of the insulator is 1×10^{-8} F/cm^2 for 300 nm SiO_2. TFT device measurements were carried out in a customized vacuum probe station ($\sim 1 \times 10^{-5}$ Torr) or in air. Coaxial and/or triaxial shielding was incorporated in a customized vacuum probe station or in a Signatone probe station (ambient measurements) to minimize the noise level. TFT characterization was performed with a Keithly 6430 subfemtoammeter and a Keithly 2400 source meter, operated by a locally written Labview program and GPIB communication. Thin films were analyzed by X-ray film diffractometry (XRD) using standard $\theta-2\theta$ techniques, with monochromated Cu Kα radiation. All $\theta-2\theta$ scans were calibrated *in situ* with the reflection of the Si (100) substrates. Films were coated with 3 nm of sputtered Au before analysis by scanning electron microscopy (SEM) using a Hitachi S4500 FE microscope.

Basic-Poly(dimethylsiloxane) (b-PDMS) Stamp Fabrication and DFHCO-4TCOp Thin-Film Conversion. PDMS (Dow Corning Sylgard 184) was prepared in an empty beaker with a 6:1 base:curing agent ratio (by weight). The materials were thoroughly mixed and then degassed in a room-temperature vacuum oven for 1.0 h or until no bubbles were visible. Next, the PDMS was 'loaded' by slow addition of finely ground Na_2CO_3 (2% by weight versus PDMS formulation) and gentle stirring to minimize trapped air bubbles. The loaded formulation was then degassed in a room-temperature vacuum oven for ∼1.0 min and then poured onto a fluorocarbon self-assembled monolayer (SAM)-coated silicon wafer in a Petri dish to a thickness of ∼10 mm. The filled Petri dish was degassed for ∼1.0 min in a room-temperature vacuum oven and then immediately placed on a hotplate preheated to 150 °C. The resulting basic-PDMS (b-PRMS) stamp was allowed to cure for ∼10 h and then detached from the silicon wafer. For **DFHCO-4TCOp** film patterning, the b-PDMS stamp was placed on the protected film such that half of the semiconducting film was covered. This substrate and the b-PDMS specimen were then held in this configuration with a 2″ binder clip and a glass slide behind the silicon substrate. A small Petri dish was next filled with aqueous HCl, and the clipped stack was placed on a hotplate set at 150 °C. After 5 min, a specially designed chamber covering the stack and the HCl container was placed on top of the hotplate, and the system was allowed to stand for 15 min. After this time, the chamber was removed, and the aqueous HCl condensation on the chamber walls was wiped off to minimize the likelihood of HCl contacting the silicon substrate. After film conversion was visually complete (0.5−1.0 h), the clipped stack was allowed to cool to room temperature before disassembly. The resulting patterned semiconductor film was finally annealed at 140 °C in a vacuum oven for 4 h prior to gold electrode deposition and FET characterization.

Computational Methods. Full geometry optimization and orbital calculations for semiconductors **1**−**6** were performed using Jaguar software with the B3LYP hybrid density functional and the 6-31G** basis set. The highest occupied (HOMO) and lowest unoccupied (LUMO) DFT orbital energies were computed. Molecular HOMOs and LUMOs were plotted using Spartan. Although HOMO and LUMO eigenvalues from density functional methods do not formally represent the ionization potential and electron affinity, there is literature precedent for their favorable agreement with experimental electron affinities, ionization potentials, and band gaps.[7c]

Results

This account begins with a discussion of synthetic strategies and routes to semiconductors **1**−**6**. Next, molecular/materials characteristics such as optical and electrochemical properties and thermal transitions as determined by UV−vis/PL spectroscopy, cyclic voltammetry, polarized optical microscopy, and DSC/TGA, are described. Solid-state microstructures and surface morphologies in the corresponding thin films as investigated by film/single-crystal X-ray diffraction and SEM are then presented. Finally, the charge transport characteristics of the **1**−**6** semiconducting films as defined in thin-film transistor configurations are discussed in the context of the other physical data.

Synthesis. The syntheses of semiconducting oligothiophenes **1**−**6** are outlined in Scheme 1. The general synthetic strategy is convergent with each building block such as peripheral (acyl/perfluoroacyl-functionalized 2-bromothiophenes) and core (5,5′-bis(tri-*n*-butylstannyl)-2,2′-dithiophenes with/without protected internal carbonyl group) units prepared independently and then Stille-coupled for the final quaterthiophene assembly. Deprotection under strongly acidic conditions was employed to prepare compounds **3** and **6**. Friedel−Crafts acylation of 2-bromothiophene affords compound **7** in 60% yield. In initial experiments, acylation was performed on thiophene, resulting in the formation of 2-hexylcarbonylthiophene in excellent yields (>80%). However, bromination of this compound under a variety of conditions invariably affords an inseparable mixture of **7** and the corresponding 3-bromo regioisomer. Finally, quaterthiophene **1** was obtained in 65% yield via Stille coupling of **7** with 5,5′-bis(tri-*n*-butylstannyl)-2,2′-dithiophene using $Pd[PPh_3]_4$ as the catalyst. An identical methodology was then used for all the thiophene−thiophene coupling reactions. The synthesis of molecule **4** began with the condensation of 2-thiophenecarboxyaldehyde with the lithium derivative of perfluoro-*n*-hexane (from 1-bromoperfluoro-*n*-hexane and *n*-BuLi) at low temperature to give alcohol **8** (∼60% yield), which was subsequently brominated at the thiophene 5-position and finally oxidized in quantitative yield to ketone **10**. Stille coupling of **10** with 5,5′-bis(tri-*n*-butylstannyl)-2,2′-dithiophene then afforded **4** in 65% yield. The synthesis of **3** and **6** follows an identical pathway. The key spirobithiophene-dioxolane (**11**) intermediate was prepared according to the multistep method reported by Brzezinski et al.[12] The bis-stannyl reagent **12** was obtained in quantitative yield by reaction of **11** with *n*-BuLi, followed by quenching

(12) Brzezinski, J. Z.; Reynolds, J. R. *Synthesis* **2002**, *8*, 1053.

Table 1. Summary of Optical Absorption Maxima, Emission Maxima, and Derived Optical Bandgaps for α4T, DH-4T, DFH-4T, and Semiconductors 1−6 in Dry THF Solution

semiconductors	absorption (λ_{max}, nm)	emission (λ_{em}, nm)	optical band gap (E_{gap}, eV)
α4T[a]	391	450, 478	2.89
DH-4T[a]	402	463, 492	2.91
DHCO-4T (1)	430	495,530	2.61
DHCO-4TCOp (2)	464	536	2.41
DHCO-4TCO (3)	408, 545[b]	520	2.18
DFH-4T[a]	398	458, 489	2.88
DFHCO-4T (4)	461	549	2.40
DFHCO-4TCOp (5)	512	590	2.21
DFHCO-4TCO (6)	452, 544[b]	495, 523	2.05

[a] From ref 7a. [b] From the longer wavelength feature with the second highest intensity.

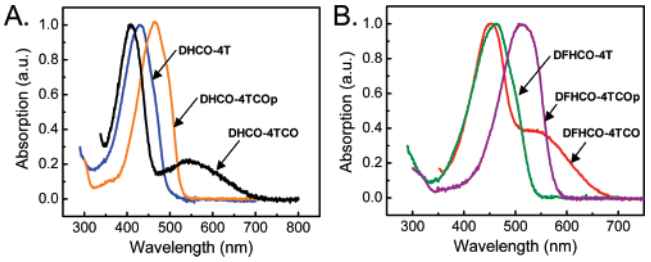

Figure 1. UV−vis spectra of (A) acyl-derivatized quaterthiophenes (**1**−**3**) and (B) perfluoroacyl-derivatized quaterthiophenes (**4**−**6**) in THF solution. Structures are labeled according to Chart 1.

with Bu_3SnCl. Stille coupling of **12** with **7** and **10** afforded **2** (63% yield) and **5** (81% yield), respectively. Finally, the dioxalane group was removed by refluxing **2** and **5** in a concentrated HCl−AcOH mixture for several minutes to afford **3** and **6**, respectively, in quantitative yields. All of the quaterthiophenes, except for **1** and **2** (recrystallization), were purified by gradient vacuum sublimation.

Optical and Electrochemical Properties. UV−vis absorption and photoluminescence (PL) spectra of semiconductors **1**−**6** were measured in solution to assess the effect of carbonyl functionalization on the optical absorption/emission spectra and resultant optical HOMO−LUMO energy gaps (E_{gap}). The optical band gap energy is determined from the onset of the long-wavelength absorption edge in the solution UV−vis spectra, and HOMO and LUMO energy levels are estimated from electrochemical data in conjunction with optical E_{gap} data. Table 1 summarizes UV−vis/PL data for all compounds in THF solution (Figures 1 and S1). The general trend in the absorption maxima is a red-shift of the $\pi-\pi^*$ transition band with chemical modification of the quaterthiophene core, in the λ_{max} ordering: 430 (**1**) < 464 (**2**) < 545 nm (**3**) in the acyl family, and 461 (**4**) < 512 (**5**) < 544 nm (**6**) in the perfluoroacyl family. Carbonyl group incorporation at peripheral locations in conjunction with hexyl and perfluorohexyl substituents induces a significant λ_{max} red-shift ($\Delta\lambda_{max}$ = +28 (**DHCO-4T**) and +63 nm (**DFHCO-4T**)) and reduction in E_{gap} (ΔE_{gap} = −0.23 (**DHCO-4T**) and −0.45 eV (**DFHCO-4T**)) compared to α,ω-di-*n*-hexylquaterthiophene, **DH-4T**, and α,ω-diperfluoro-*n*-hexylquaterthiophene, **DFH-4T**. Such large changes in optical properties are directly attributed to the effective conjugation of the peripheral carbonyl groups with the oligothiophene core π system. Note that similar red-shift in λ_{max} due to the extended conjugation has been observed previously for formyl[13] and ester[14] end-capped quaterthiophenes. Furthermore, the additional C=O group in the **DHCO-4TCO** and **DFHCO-4TCO** cores further enhances the red-shifts in the absorption maxima by extending the conjugation, thereby significantly compressing the optical band gap compared to **DHCO-4T** (ΔE_{gap} = −0.43 eV) and **DFHCO-4T** (ΔE_{gap} = −0.35 eV), respectively.[15] Although there is no additional π-electron donation for the case of dioxolane core modification in **DHCO-4TCOp** and **DFHCO-4TCOp**, holding the innermost bithiophene fragment in a *syn* conformation reasonably contributes to the decrease in E_{gap} by planarizing the conjugated core. Indeed, the very flat core structure of semiconductor **3** was confirmed by single-crystal X-ray diffraction (*vide infra*).

Table 2. Summary of Electrochemical Reduction/Oxidation Potentials and the Corresponding LUMO/HOMO Energies of α4T, DH-4T, DFH-4T, and Semiconductors 1−6 in Dry THF

semiconductor	$E_{1/2,Red}$ (V)	$E_{1/2,Ox}$ (V)	LUMO[a] (eV)	HOMO[b] (eV)
α4T[c]	−1.94		−2.90	−5.79
DH-4T[c]	−1.95	0.96	−2.89	−5.80
DHCO-4T (1)	−1.06		−3.78	−6.34
DHCO-4TCOp (2)	−1.45	1.12	−3.39	−5.79 (−5.96)
DHCO-4TCO (3)	−0.84	1.31	−4.00	−6.16 (−6.15)
DFH-4T[c]	−1.53	1.35	−3.31	−6.19 (−6.19)
DFHCO-4T (4)	−0.88		−3.96	−6.33
DFHCO-4TCOp (5)	−1.20	1.42[d]	−3.64	−5.61
DFHCO-4TCO (6)	−0.65		−4.19	−6.05

[a] LUMO energy estimated from the following relationship: LUMO (eV) = −4.84 eV − e $E_{1/2,Red}$, ref 15. [b] HOMO energy estimated from the following relationship: HOMO (eV) = LUMO - E_{gap}. Numbers in parentheses indicate HOMO energies estimated using $E_{1/2,ox}$. [c] Reference 7b. [d] Irreversible.

Particularly interesting is the comparison of the optical spectra of the acyl and perfluoroacyl families. As previously reported, the absorption and emission spectra of **DH-4T** and **DFH-4T** in solution are very similar to those of quaterthiophene (α4T), and, consequently, their optical band gap energies fall in the same range (2.80−2.89 eV) although their HOMO and LUMO energies are substantially modulated by the α,ω-*n*-hexyl and perfluoro-*n*-hexyl substituents (Table 2).[6b] In contrast, E_{gap} reduction by carbonyl group introduction is significantly more pronounced in the perfluoroacyl series than in the acyl series, implying that extending the core conjugation is more effective from the combination of perfluoroalkyl and carbonyl substituents than for the combination of alkyl and carbonyl substituents.

The electrochemical properties of semiconductors **1**−**6** reveal important electronic structure-materials performance trends.[16,17] Cyclic voltammetry (CV) studies were performed in 0.1 M TBAPF solutions in THF with scan rates ~100 mV/s, and the formal potentials ($E^{1/2}$) were extracted as the midpoints between the peak potentials of the forward and

(13) Wei, Y.; Yang, Y.; Yeh, J.-M. *Chem. Mater.* **1996**, *8*, 2659.
(14) DiCesare, N.; Belletete, M.; Donot-Bouillud, A.; Leclerc, M.; Durocher, G. *Macromolecules* **1998**, *31*, 6289.
(15) Dal Colle, M.; Cova, C.; Distefano, G.; Jones, D.; Modelli, A.; Comisso, N. *J. Phys. Chem.* **1999**, *103*, 2828.
(16) Bard, A. J.; Faulkner, L. R. *Electrochemical Methods-Fundamentals and Applications*; Wiley: New York, 1984; p 634.
(17) (a) Domagala, W.; Laokowski, M.; Guillerez, S.; Bidan, G. *Electrochim. Acta* **2003**, *48*, 2379. (b) Renak, M. L.; Bartholomew, G. P.; Wang, S.; Ricatto, P. J.; Lachicotte, R. J.; Bazan, G. C. *J. Am. Chem. Soc.* **1999**, *121*, 7787.

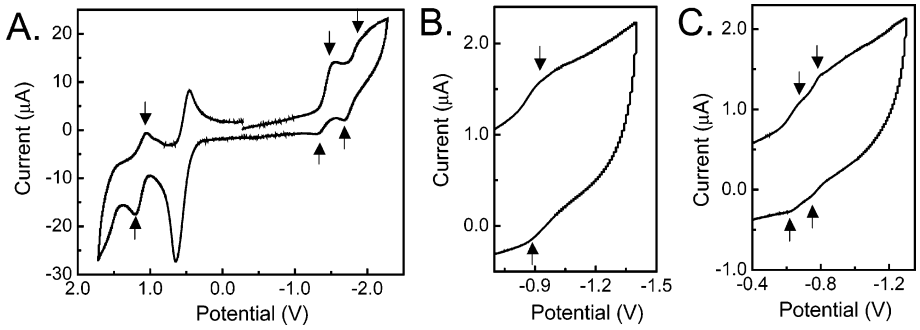

Figure 2. Representative cyclic voltammograms of oligothiophenes: (A) **DHCO-4TCOp**, (B) **DFHCO-4T**, and (C) **DFHCO-4TCO**. Measurements were performed in 0.2 M TBAPF in THF at a scan rate 100 mV/s. Horizontal axis is normalized to $E_{1/2}$ (Fc/Fc$^+$) = +0.54 V. The arrows denote oxidation/reduction peaks. Structures are labeled according to Chart 1.

reverse scans with respect to a ferrocene reference (+0.54 V vs. SCE in THF). Selected cyclic voltammograms of **DHCO-4TCOp**, **DFHCO-4T**, and **DFHCO-4TCO** are shown in Figure 2. All quaterthiophene systems exhibit two reversible and/or quasi-reversible one-electron reduction peaks, while **DHCO-4TCOp** and **DFHCO-4TCOp** exhibit two reversible peaks in both reduction and oxidation. The electrochemical data are summarized in Table 2. Upon carbonyl group introduction, first reduction potentials increase in the following order: −1.95 (**DH-4T**) < −1.06 (**DHCO-4T**) < −0.84 V (**DHCO-4TCO**), consistent with the trend that increasing numbers of electron-withdrawing/delocalizing carbonyl substituents correlate with a monotonic increase in reduction potential. Note also that any additional reduction potential depression from **DHCO-4T** to **DHCO-4TCO** ($\Delta E_{1/2}$ = 0.22 V) due to the introduction of an additional molecular core carbonyl group is much less pronounced than the reduction potential change per peripheral carbonyl substituent from **DH-4T** to **DHCO-4T** ($\Delta E_{1/2}/2$ = 0.45 V), implying that carbonyl substitution has less of an effect in the quaterthiophene core than at the periphery. This observation is fully supported by DFT computations of the frontier molecular orbitals (*vide infra*). More striking is the decrease in reduction potential on proceeding from **DHCO-4T** to **DHCO-4TCOp**. While two acyl functionalities still reside in the molecular structure and the oligothiophene conjugated core geometry is locked in a planar conformation, the dioxolane group is clearly electron-donating and cancels the acyl substituent electron-withdrawing effects.

Very similar correlations between electrochemical data and substituent effects are observed in the perfluoroacyl oligothiophene family. Enhanced electron-withdrawing/delocalizing effects with increased numbers of carbonyl functionalities are manifested in the gradual increase in reduction potential in the following order: −1.53 (**DFH-4T**) < −0.88 (**DFHCO-4T**) < −0.65 V (**DFHCO-4TCO**). In contrast, the dioxolane group perturbation of electron-withdrawing capacity in **DFHCO-4TCOp** induces a drastic deviation from the general $E_{1/2,\mathrm{Red}}$ − carbonyl substitution trend.

Thermal Properties of Semiconductors 1−6. Melting points and transition temperatures from differential scanning calorimetry (DSC) measurement are summarized in Table 3. Compared to the analogues without acyl groups (**DH-4T** and **DFH-4T**), acyl end-capped **DHCO-4T** and **DFHCO-4T** exhibit much higher melting points. Although there is a molecular weight increase (~60 amu) on insertion of carbonyl groups between the oligothiophene core and alkyl/fluoroalkyl chains, it is suggested that intermolecular dipole−dipole and $\pi-\pi$ interactions are enhanced by the extended intramolecular conjugation due to the polar carbonyl groups, and a similar effect is evident in the aldehyde end-capped quaterthiophene which exhibits a far higher melting point (~270 °C) than α-quaterthiophene (216 °C).[13] Interestingly, this effect is more substantial in **DHCO-4T** (ΔT_{mp} = 106 °C) than in **DFHCO-4T** (ΔT_{mp} = 35 °C), leading to a reversed ordering of melting points. In the case of moderate core-size oligothiophenes (e.g., quaterthiophenes), the melting points of diperfluoroalkyl-substituted analogues are substantially higher than those of the dialkyl-substituted analogues.[7b] The reason for this unusual inversion in melting point trend with carbonyl incorporation is not immediately evident but can be attributed to the possible different solid-state packing characteristics in **DHCO-4T** and **DFHCO-4T**. In contrast, for **DHCO-4TCOp** and **DFHCO-4TCOp**, the melting points decrease significantly and approach those of non-carbonyl analogues (**DH-4T** and **DFH-4T**). This appears to arise from unfavorable intermolecular core interactions, possibly caused by the bulky dioxolane protecting group. When the third carbonyl group is introduced in the quaterthiophene core, in addition to the peripheral acyl functionalization, the melting points further increase to 260 °C for **DHCO-4TCO** and 297 °C for **DFHCO-4TCO**, indicating larger/broader core conjugation and stronger solid-state intermolecular attractive interactions. Note that in addition to the extended conjugation, such a bridging carbonyl substituent which holds the innermost bithiophene

Table 3. Summary of Melting Point and DSC/TGA Transition Temperature Data for DH-4T, DFH-4T, and Semiconductors 1−6

		T_{DSC} (°C)		
semiconductors	mp (°C)	heating	cooling	T_{TGA}[a] (°C)
DH-4T[b]	184	88, 186	178, 42	184
DHCO-4T (1)	290	243, 290	287, 239	287
DHCO-4TCOp (2)	180	290	172	309
DHCO-4TCO[c] **(3)**	260	278		297
DFH-4T[b]	213	213	203	153
DFHCO-4T (4)	248	245, 248	244, 234	204
DFHCO-4TCOp (5)	218	224	207	246
DFHCO-4TCO (6)	297	301	267	255

[a] Calculated as the temperature where 2% of the material has sublimed at a constant ~5 Torr and a ramp rate of 2 °C/min. [b] Data from ref 7b. [c] Irreversible DSC cycle.

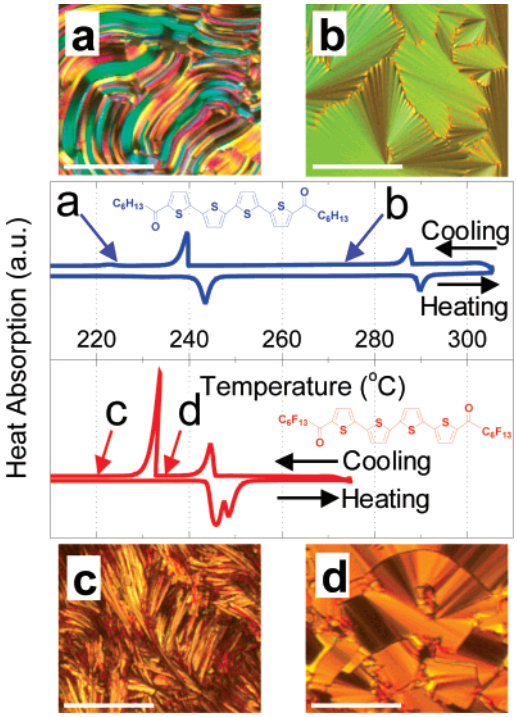

Figure 3. Center: DSC scans of **DHCO-4T** (blue) and **DFHCO-4T** (red), and polarized optical images of **DHCO-4T** (**a**: 225 °C, **b**: 273 °C) and **DFHCO-4T** (**c**: 220 °C, **d**: 235 °C) in the second cooling cycle. Images taken under 90° cross-polarization conditions. Scale bars denote 200 μm.

in a *syn* conformation breaks the C_2 symmetry in both acyl- and perfluoroacyl quaterthiophenes, and the resulting structures with three carbonyl groups aligned in one direction induce a relatively large dipole moment, estimated as ~5 Debyes for both **DHCO-4TCO** and **DFHCO-4TCO** by DFT calculations, in contrast to <0.1 D for DHCO-4T and DFHCO-4T (*vide infra*). Note that recent studies demonstrate that dipole moments can be calculated with good accuracy by DFT methods.[18] Therefore, it is suggested that the intermolecular dipole−dipole interactions contribute to the additional increase in **DHCO-4TCO** and **DFHCO-4TCO** melting points and that their packing motifs likely differ from those of **DHCO-4T** and **DFHCO-4T** which do not have large dipole moments and assume core quaterthiophene all-trans conformations.

The comparative thermal behavior of semiconductors **1**−**6** was further investigated by differential scanning calorimetry (DSC) and thermogravimetric analysis (TGA). The present DSC scans were performed under nitrogen at heating and cooling rates of 5 °C/min. Compounds **1** and **2** and **4**−**6** exhibit reversible cycles, and DSC scans were collected in the second cycle (Figures 3 and S2). While **DHCO-4TCO** exhibits only a single endothermic transition on heating, the DSC data reveal that semiconductors **1** and **4** undergo multiple thermal transitions (Figure 3). In the heating cycle, both **DHCO-4T** and **DFHCO-4T** exhibit the first/second endothermic features at 243/290 °C and 245/248 °C, respectively.

To investigate the existence of liquid crystal (LC) phases in these compounds, polarized optical micrographs were acquired during the cooling cycle (Figure 3). Upon passing the first exothermic transitions with a very slow cooling rate of 0.1 °C/min, the data for both compounds reveal that the **DHCO-4T** isotropic phase (liquid) disappears and that an anisotropic mesophase separates from the liquid. The textures of both compounds in the LC phase are reminiscent of smectic liquid crystals.[19] As partly indicated in the melting point trend from **DH-4T**/**DFH-4T** to **DHCO-4T**/**DFHCO-4T**, incorporation of the acyl groups improves intermolecular packing and possibly enforces long-range ordering, which is reflected by the presence of an LC phase. Since charge transport in organic semiconductors is substantially affected by intermolecular $\pi-\pi$ interactions, the existence of such kinds of mesophases might be utilized to further align the semiconducting layers by thermal treatment and abrupt quenching.[20]

Semiconductors **1** and **4**−**6** all sublime cleanly and quantitatively at ~5 Torr, while semiconductors **2** (**DHCO-4TCOp**) and **3** (**DHCO-4TCO**) leave some residue due to possible decomposition, as shown in TGA scans (Figure S3). In general, perfluoroalkyl-terminated oligothiophenes are thermally more stable and sublime without any residue at lower temperatures than the alkyl-terminated analogues,[6] and the same trend is preserved in the present carbonyl-functionalized alkyl/perfluoroalkyl quaterthiophene families. Such enhanced thermal stability and volatility are favorable for film growth from the vapor phase, which, in turn, leads to more reproducible device fabrication without artifacts/contamination by impurities or decomposition byproducts.

DFT B3LYP Electronic Structure Calculations. To understand the optical/electrochemical trends observed upon carbonyl functionalization of the quaterthiophene core, DFT/B3LYP electronic structure computations at the 6-31G** basis set level of theory were performed on semiconductors **1**−**6**. The spatial representations of the HOMO and LUMO frontier orbitals are shown in Figure 4. Clearly, while the HOMOs of **1**−**6** exhibit similar spatial characteristics, the LUMO topologies vary within the series. Furthermore, the HOMOs exhibit poor conjugation between the thiophene central portion and the carbonyl fragments, probably because the n_{CO} and core filled π orbitals cannot interact for symmetry reasons. The result is the presence of nodal planes between the lateral C═O groups and the oligothiophene core for **1** and **4**, whereas in the case of central C═O insertion in **DFHCO-4TCO** and **DHCO-4TCO**, the nodal plane bisects the C═O group. On the other hand the LUMOs of **1**−**6** fully extend to the carbonyl groups. Note that for semiconductors **2** and **5,** in which the dioxolane moiety breaks the conjugation, the HOMO/LUMO topographies are similar to those

(18) Pitonak, M.; Holka, F.; Neogrady, P.; Urban, M. *THEOCHEM* **2006**, *768*, 79.

(19) (a) Funahashi, M.; Tamaoki, N. *Chem. Mater.* **2007**, *19*, 608. (b) Toba, M.; Takeoka, Y.; Rikukawa, M. *Synth. Met.* **2003**, *135*−*136*, 339. (c) Ponomarenko, S.; Kirchmeyer, S. *J. Mater. Chem.* **2003**, *13*, 197. (d) Rosu, C.; Manaila-Maximean, D.; Paraskos, A. J. *Mod. Phys. Lett. B* **2002**, *16*, 473. (e) Sharma, S.; Lacey, D.; Wilson, P. *Liq. Cryst.* **2003**, *30*, 461. (f) Liu, P.; Nakano, H.; Shirota, Y. *Liq. Cryst.* **2001**, *28*, 581. (g) Yamada, T.; Azumi, R.; Tachibana, H.; Sakai, H.; Abe, M.; Baüerle, P.; Matsumoto, M. *Chem. Lett.* **2001**, *30*, 1022. (h) Funahashi, M.; Hanna, J. *Appl. Phys. Lett.* **2000**, *76*, 2574. (i) Azumi, R.; Götz, G.; Baüerle, P. *Synth. Met.* **1999**, *101*, 544.

(20) Melucci, M.; Gazzano, M.; Barbarella, G.; Cavallini, M.; Biscanini, F.; Maccagnani, P.; Ostoja, P. *J. Am. Chem. Soc.* **2003**, *125*, 10266.

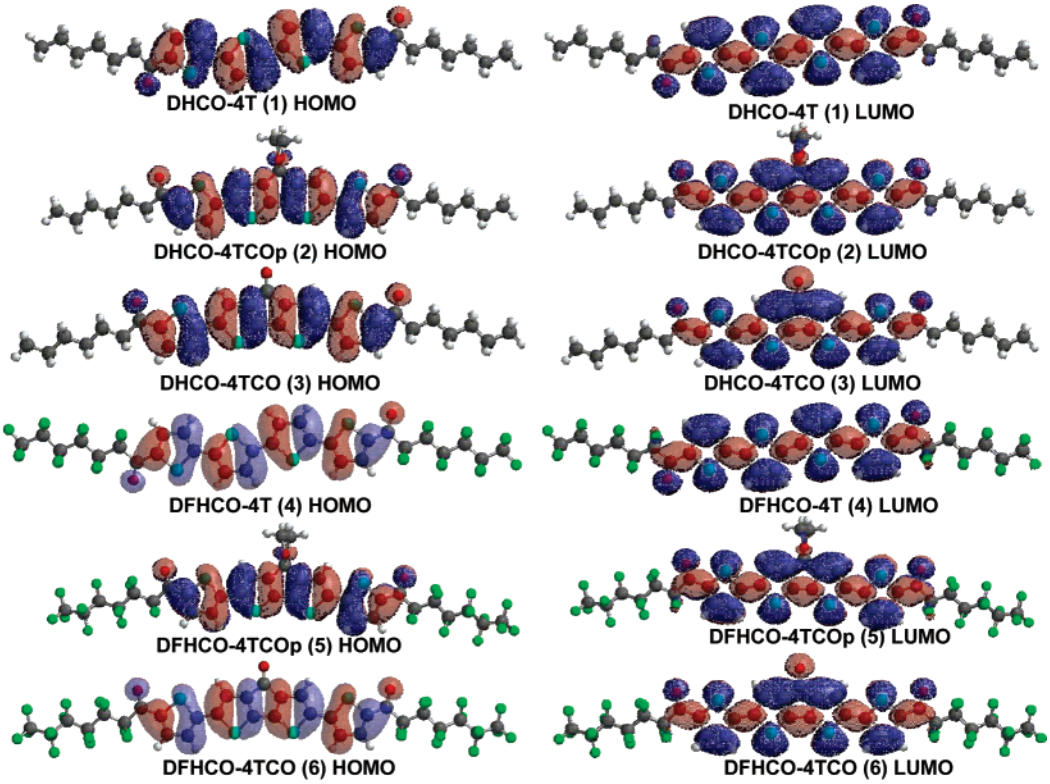

Figure 4. Frontier molecular orbitals of semiconductors **1**−**6** calculated using DFT/ B3LYP and the 6-31G** basis set.

Table 4. Summary of DFT Derived HOMO and LUMO Energies of α4T, DH-4T, DFH-4T, and Semiconductors 1−6

semiconductor	HOMO (eV)	LUMO (eV)	E_{gap} (eV)	dipole moment (D)
α4T[a]	−4.95	−1.93	3.02	0.020
DH-4T[a]	−4.76	−1.80	2.97	0.005
DHCO-4T (1)	−5.33	−2.60	2.73	0.71
DHCO-4TCOp (2)	−5.15	−2.57	2.58	3.80
DHCO-4TCO (3)	−5.45	−3.09	2.36	8.42
DFH-4T[a]	−5.58	−2.39	3.18	1.418
DFHCO-4T (4)	−5.90	−3.12	2.78	0.00
DFHCO-4TCOp (5)	−5.64	−3.20	2.45	1.00
DFHCO-4TCO (6)	−5.95	−3.57	2.38	5.60

[a] Reference 7b.

of the corresponding dicarbonyl-substituted semiconductors **1** and **4**.

The calculated HOMO and LUMO eigenvalues and dipole moments of the present semiconductors are compiled in Table 4. Energetic variations are in accord with the HOMO/LUMO topographies of Figure 4, where the carbonyl groups are fully involved with the LUMOs but marginally contribute to the HOMOs. The result is a greater LUMO vs. HOMO energy reduction and consequent greater LUMO stabilization, greater electron accepting capacities, and reduced bandgaps of the carbonyl-containing oligothiophene derivatives compared to **DH-4T** and **DFH-4T**. Indeed, on going from **α4T**/**DH-4T** → **1**, **3** and α4T/**DFH-4T** → **4**, **6** the LUMO energies decrease by ∼2× (1.3−1.7 eV) compared to the HOMO (0.7−1.0 eV) energies. Consequently, the computed energy gaps are reduced from ∼ 3 eV for α4T/**DH-4T**/**DFH-4T** to ∼2.7−2.8 eV for **1**/**4** (two carbonyl-containing semiconductors) to ∼2.4 eV for **3**/**6** (three carbonyl-containing semiconductors) in agreement with experimental physiochemical data (see below). Similar trends were reported by Distefano and co-workers for oligo(2-thienylene ketone)s, in which the computed HOMO and LUMO trends were confirmed in ionization potential and electron affinity determinations via UPS and ET spectroscopy.[21]

The present DFT-computed HOMO/LUMO energy trends are in agreement with the experimental electrochemical and optical data where the energy gaps and the LUMO levels are significantly depressed with increasing numbers of carbonyl groups (Tables 1, 2, and 4). Furthermore, the experimentally derived HOMO energies confirm that they are generally much less affected by carbonyl introductions, as predicted by the theory. Interestingly, the electrochemically derived HOMO/LUMO energies of dioxolane semiconductors **2** and **5** do not follow the trends predicted by DFT. Based on the results from the DFT calculations, **2** and **5** can be treated as two-carbonyl systems, therefore explaining why their LUMO energies are very similar (energy differences <0.1 eV) to those of **1** and **4**. However, experimentally we find that the LUMO energies of **2** and **5** are much greater (>0.3 eV) than those of **1** and **4,** and this could be due to conformational effects and/or solvation not taken into account in these calculations.

Single-Crystal Structures. Single crystals of the new oligomer **DHCO-4TCOp** were grown by slow cooling of saturated xylene solutions, and the crystal structure determined by X-ray diffraction is shown in Figure 5A. The quaterthiophene core is substantially planar and exhibits maximum torsional angles between the cyclopentadithiophenone and the peripheral thiophene rings of 5.7 and 6.0°. These angles are comparable to those observed in planar

(21) Dal Colle, M. C.; Distefano, G.; Jones, D.; Modelli, A.; Comisso, N. *J. Phys. Chem. A* **1999**, *103*, 2828.

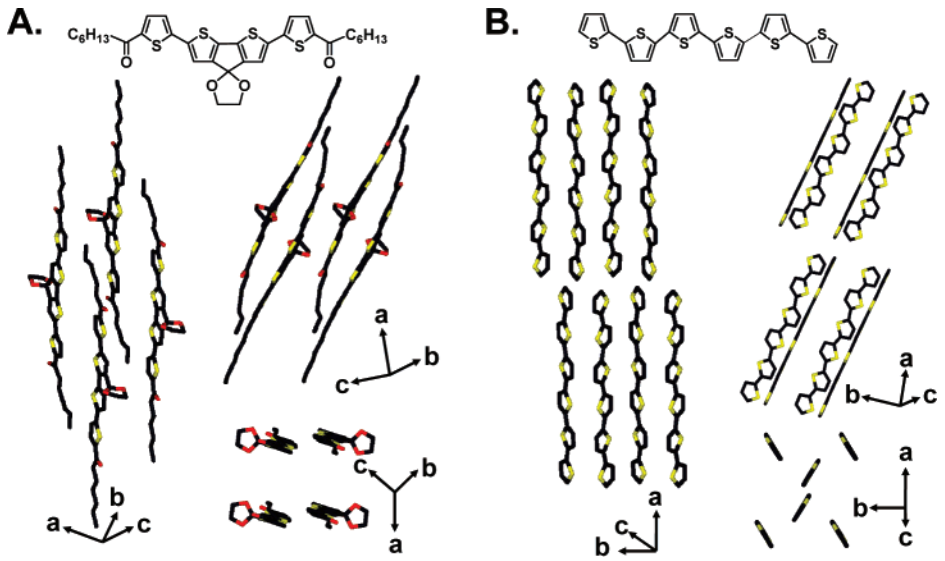

Figure 5. Single-crystal structures of A. **DHCO-4TCOp** and B. α-sexithiophene (from the Cambridge Crystallographic Database).

α-sexithiophene (4.1°)[22] and in **DFH-4T** (<2°).[7b] The α,ω-carbonyl groups lie in the quaterthiophene core plane, and the alkyl substituents are extended along the molecular long axes. Although the overall molecular shape approximates a rod with a molecular long-axis length of 32.7 Å, it is evident that the dioxolane group induces relatively large sterically based intermolecular separations along the direction parallel to the molecular planes. Particularly interesting is the molecular packing motif. In contrast to typical oligothiophene herringbone stacking with long axis twist angles of 60−70° (compare in Figure 5B),[22] the crystal structure of **DHCO-4TCOp** exhibits $\pi-\pi$ cofacial packing. Such an arrangement resembles the parallel $\pi-\pi$ stacking found in single crystals of arenes having both electron-rich and electron-deficient subunits.[8,6a] Note that such cofacial arrangements enhance intermolecular π orbital overlap and should therefore decrease the barrier to charge transport versus a herringbone packing motif. The minimum interplanar distance between cofacial **DHCO-4TCOp** molecules is 3.42 Å (C_9-C_{19}'), very similar to that found for alkyl- and perfluoroalkyl oligothiophenes (∼3.5 Å).[7b] This relatively short intermolecular distance is surprising considering the presence of the bulky oxolane protecting group located in the molecular core center. The molecules are partially interdigitated along the molecular long-axes, extending away from the *ac*-plane, with the closest neighboring conjugated cores in cofacial registry by only ∼60%. This slipped cofacial stacking reduces nonbonded repulsion between neighboring dioxolane substituents. Another distinctive feature of the **DHCO-4TCOp** crystal structure is the antiparallel dioxolane orientation in nearest-neighbor cofacial molecular pairs. This interesting arrangement may be explained by arguments considering the molecular dipole moment arrangements in the **DHCO-4TCOp** lattice. The *anti-syn-anti* conformation allows the two carbonyl substituents to align in parallel, resulting in a net molecular dipole moment. Therefore, it is suggested that antiparallel alignment of nearest neighbor $\pi-\pi$ stacked molecules avoids in-parallel dipole−dipole repulsion and contributes to overall minimization of the lattice energy.

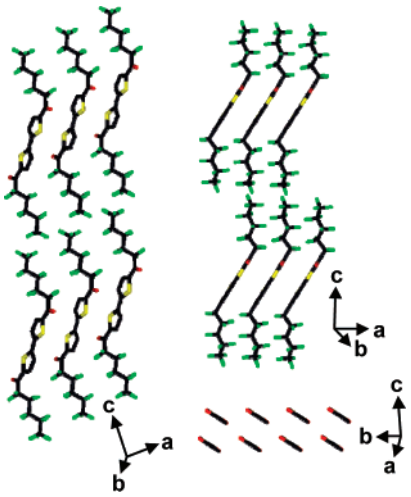

Figure 6. Single-crystal structure and packing of **DFPCO-2T**.

Unfortunately, it was not possible to obtain diffraction-quality single crystals of semiconductors **4**−**6**. Instead, single crystals of diperfluoropentylcarbonylbithiophene (**DFPCO-2T**), which is a shorter oligomer analogoue to **DFHCO-4T**, were obtained as a byproduct in the synthesis of diperfluorohexybithiophene (**DFH-2T**, **7**),[7a]

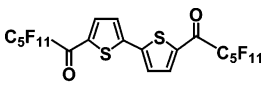

DFPCO-2T (7)

and the crystal structure determined by X-ray diffraction is shown in Figure 6. The bithiophene core is substantially planar with maximum torsional angles between the two *anti* thiophene rings of <1.0°. The α,ω-carbonyl groups lie in the bithiophene core plane; however, in contrast to **DHCO-4TCOp** with alkyl chains stretched along the molecular long axis in a gauche conformation, the perfluoroalkyl substituents in **DFPCO-2T** exhibit a zigzag helical conformation characteristic of fluorocarbon chains[23] and are positioned at ∼145° with respect to the bithiophene backbone axis. Unlike

(22) Fichou, D. *J. Mater. Chem.* **2003**, *10*, 571 and references therein.

(23) Bunn, C. W.; Howells, E. R. *Nature* **1954**, *174*, 549.

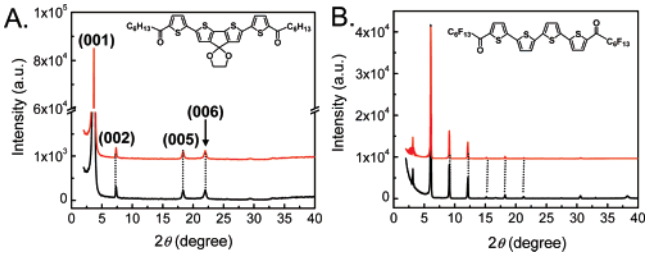

Figure 7. Representative XRD $\theta-2\theta$ scans of (A) **DHCO-4TCOp** and (B) **DFHCO-4T**. Black (bottom) and red (top) plots represent scans of films deposited at the substrate temperatures of 25 and 70 °C, respectively. Bragg progression peaks in the **DHCO-4TCOp** film are assigned from the single-crystal structure data.

the solid-state herringbone stacking in perfluoroalkyl-derivatized oligothiophenes,[7b] the crystal structure of **DFPCO-2T** exhibits slipped $\pi-\pi$ cofacial packing, and the minimum interplanar distance between cofacial molecules in adjacent planes is 3.63 Å (S_1-S_1'). Note that this slipped cofacial stacking reduces the unfavorable parallel carbonyl dipole−dipole interactions. Considering the typical enhancements in conjugated core−core interactions typically observed with increased thiophene core size,[7b] e.g., from bithiophene to quater- to sexithiophene, it is expected that cofacial stacking at minimal interlayer distances is preserved perfluoroalkylcarbonyl-derivatized quaterthiophenes **4**−**6**.

Film Microstructure and Morphology. X-ray diffraction (XRD) and scanning electron microscopy (SEM) were performed to investigate microstructures and morphologies of the films of semiconductors **1**−**6**. These were characterized as ∼50 nm films, vacuum-deposited on HMDS-treated p^+-Si/SiO_2 substrates. Table 4 summarizes *d*-spacings (*d*) extracted from Bragg progression reflections in conventional $\theta-2\theta$ scans, computed molecular long-axis lengths (*l*),[24] and tilt angles (φ) with respect to the substrate normal, calculated from the *d* and *l* data assuming solid-state layer packing similar to **DFPCO-2T** and other (perfluoro)alkyloligothiophenes. The XRD scans show that all films are highly textured when grown both at substrate temperatures of 25 and 70 °C. Representative XRD scans are shown in Figure 7. All diffraction scans exhibit single dominant Bragg progressions, and the peak profiles in films grown at 25 and 70 °C are essentially identical, with only minor differences in relative intensity patterns.

In the case of the fluorine-free acyl oligothiophenes, very similar *d*-spacings are observed for films of **DHCO-4T** and **DHCO-4TCO** (Figure S4). The molecular or long axis tilt angles with respect to the surface normal defined from *d*-spacings and computed molecular lengths are very close to 0°, indicating that the **DHCO-4T** and **DHCO-4TCO** molecules are oriented almost perpendicular to the surface plane and that such edge-on molecular orientation is preserved despite the bridging-carbonyl presence in the oligothiophene core. In contrast to **DHCO-4T** and **DHCO-4TCO**, the **DHCO-4TCOp** films exhibit substantial inclination in molecular orientation with an estimated long axis tilt angle of ∼42°. Indeed, these data and the single-crystal

(24) Calculations of the optimized geometries of semiconductors **1**−**6** were performed using Jaguar/DFT-B3LYP with a HF 6-31G** basis set.

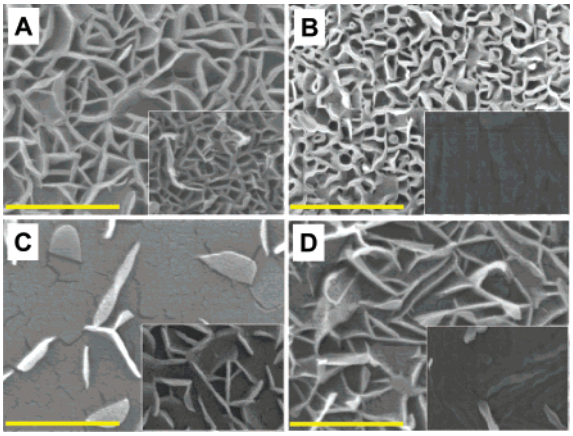

Figure 8. SEM images of (A) **DHCO-4T** (70 °C), **DHCO-4T** (25 °C, inset), (B) **DHCO-4TCO** (70 °C) and **DHCO-4TCOp** (70 °C, inset), (C) **DFHCO-4T** (70 °C), **DFHCO-4T** (25 °C, inset), and (D) **DFHCO-4TCO** (70 °C) and **DFHCO-4TCOp** (70 °C, inset). All scale bars represent 1 μm and also apply to the inset images. Substrate growth temperatures are given in parentheses.

structure of **DHCO-4TCOp** confirm that the angle between the molecular long-axis and the surface normal of the crystal *ac* plane is essentially identical to the calculated thin-film molecular tilt angle, indicating that the out-of-plane molecular orientation in the vapor-deposited thin films parallels that in the crystal structure.

Considering the similarity in DFT-computed geometric structures of the acyl and perfluoroacyl oligothiophenes (Figure S3) and the similar trends in optical and electrochemical properties of both families, it is reasonable to assume rodlike molecular geometries with essentially planar oligothiophene cores and linearly extended perfluoroacyl substituents for all members of the series. Perfluoroacyl-derivatized oligothiophenes exhibit similar film microstructure trends as in their acyl-derivatized counterparts upon bridged dioxolane and carbonyl incorporation into the respective oligothiophene cores. XRD scans of the **DFHCO-4T** and **DHCO-4TCOp** films reveal sharp Bragg reflection progressions up to seventh order diffraction, and each progression corresponds to a single phase with *d*-spacings of 29.1 and 30.2 Å, respectively (Figure 7). The estimated tilt angles of these molecular structures are similar to that of **DFH-4T** (∼25°), strongly suggesting an edge-on molecular orientation on the substrate surface with a modest inclination. In contrast, for **DFHCO-4TCOp** films, the molecules are significantly inclined toward the substrate plane with an estimated tilt angle ∼60°, even greater than that of the inclined acyl analogue (**DHCO-4TCOp**), although a single Bragg progression is observed. It is plausible to argue that the protruding protecting group causes the solid-state packing to differ significantly from those of **DFHCO-4T** and **DFHCO-4TCO** for the same reason as for **DHCO-4TCOp**.

SEM images were recorded to examine the morphologies of the **1**−**6** semiconducting films grown from the vapor phase at 25 and 70 °C. As can be seen in Figure 8, these films display morphological features such as embedded vertical ridges, interconnected honeycomb-like walls, ribbonlike tapes, and amorphous smooth surfaces. The **DHCO-4T** and **DHCO-4TCO** films exhibit similar overall morphologies

such as highly interconnected honeycomb-like walls. Such films deposited on 70 °C substrates exhibit larger grains/vertical walls than those deposited on 25 °C substrates. Interestingly, although XRD scans of the **DHCO-4TCOp** films exhibit a single family of Bragg progressions, the morphology is that of a completely featureless smooth surface for 25 °C substrate growth and a similarly smooth surface with leafy embedded rods for 70 °C growth.

In contrast to the above observations, the effects of chemical substituents on film morphologies in several of the perfluoroacyl oligothiophenes are considerably different from those in the acyl oligothiophene series. Thus, **DFHCO-4T** films exhibit interconnected vertical ridges embedded on the smooth surfaces in the case of specimens grown at 25 °C. However, when the substrate temperature is increased, the film morphology becomes smoother, and most of vertical ridges are isolated; at higher magnification, pits and long cracks are evident on the surface. In case of **DFHCO-4TCOp** films, the SEM images reveal relatively smooth morphologies with random stacking of planar ribbon-like tapes, very similar to films of the carbonyl-protected **DHCO-4TCOp** counterpart. However, at higher growth temperatures, far smoother morphologies are observed in the latter with coalescence of these tapes. The **DFHCO-4TCO** films exhibit crystalline morphologies upon removal of the bulky protecting group, and elevated growth temperatures induce larger grains and vertical ridges as in the acyl oligothiophene series.

Thin-Film Transistor Device Characterization

Top contact thin-film transistors of semiconductors **1**−**6** were fabricated in the manner described in the Experimental Section. All films were vacuum-deposited on HMDS-treated SiO_2/p^+-Si substrates maintained at temperatures (T_D) of either 25 or 70 °C, and TFT fabrication was completed by evaporating gold through a shadow mask to define the source and drain electrodes. All measurements were performed under vacuum at a temperature of 25 °C, and to derive representative metrics of performance parameters in each semiconductor device set, at least 3−5 devices were tested at spatially different regions over each OTFT set, and the average is reported. Transistor response data were analyzed using standard field-effect transistor equations.[25] When the current I_{DS} saturates at large V_{DS}, mobility and other parameters are related by the following relationship: $\mu_{sat} = (2I_{DS}L)/[WC_{ox}(V_G-V_T)^2]$ where L and W are the device channel length (100 μm) and width (5 mm), respectively, and C_{ox} (10 nF/cm^2) is the gate oxide capacitance. The mobility (μ) and threshold voltage (V_T) can then be calculated from the slope and intercept, respectively, of the linear part of the V_G vs. $(I_{DS})^{1/2}$ plot (at $V_{DS} = 100$ or -100). Mobility, threshold voltage, and current on−off ratio data for OTFTs based on semiconductors **1**−**6** are summarized in Table 6.

The first OTFT observation to be made is that all films of the **1**−**6** series are field-effect transistor active, independent of the chemical functionalization and film growth temperature. It was found that **DHCO-4T** exhibits ambipolar activity with appreciable electron (0.12 cm^2/Vs) and hole (0.008 cm^2/Vs) mobilities at the substrate growth temperature of 70 °C, and **DFHCO-4T** shows monopolar n-type activity with an exceptionally high mobility of 0.32 cm^2/Vs for semiconducting films deposited at a substrate temperature of 25 °C.[9] Note that similar carbonyl group effects on n-type (electron) transport were previously demonstrated in electroactive aromatic polyketones and polyesters.[26] Upon additional carbonyl group introduction into the quaterthiophene core, **DFHCO-4TCO** exhibits stable n-type activity even in the air although the observed electron mobility in the air (0.01 cm^2/Vs) is somewhat lower than that under vacuum (0.08 cm^2/Vs). Recently, after proper dielectric surface modification in interfacial studies reported elsewhere, n-type mobilities were substantially improved: values up to 0.67 cm^2/Vs for **DHCO-4T** and 1.7 cm^2/Vs for **DFHCO-4T** were measured.[27] Note that these values are among the highest n-type mobilities reported in the literature,[6f] and, in the following, we extend our study to the full electrical characterization of semiconductors **1**−**6**, probing the interplay of chemical functionality and transistor device characteristics.

Table 5. Summary of Diffraction-Derived *d*-Spacings (*d*), DFT Computed Molecular Lengths (*l*), and Calculated Molecular Long Axis Tilt Angles in Semiconducting Films (50 nm) of Compounds 1−6

semiconductor	*d*-spacing (*d*, Å)	molecular length (*l*, Å)	tilt angle[a] (φ, °)
DH-4T[b]	28.5	33.7	32
DHCO-4T	34.3	33.6	∼0
DHCO-4TCOp	24.3	33.7	44
DHCO-4TCO	33.2	33.6	∼0
DFH-4T[b]	29.4	32.4	25
DFHCO-4T	29.1	34.1	31
DFHCO-4TCOp	17.1	33.8	60
DFHCO-4TCO	30.2	34.1	28

[a] With respect to the substrate normal. $\varphi = \cos^{-1}$ (d/l). [b] Data from ref 7a.

OTFT activities of acyl oligothiophenes **1**−**3** were examined after growth at two different substrate temperatures, 25 and 70 °C (Figure 9). In case of ambipolar **DHCO-4T** films grown at 70 °C, both n- and p-type mobilities as well as current on−off ratios are enhanced by orders of magnitude compared to films grown at 25 °C, indicating that in contrast to **DFHCO-4T** films, the substrate temperature plays an important role in improving both electron- and hole-transport. Although **DHCO-4TCOp** has the same core and side-chain molecular structure as **DHCO-4T**, except that dioxolane functionality fixes the innermost bithiophenes in a *syn* conformation, the TFT response data reveal very different electrical behavior compared to **DHCO-4T** TFT. Interestingly, **DHCO-4TCOp** exhibits *only* p-type activity, with no detectable n-type behavior. Hole mobility extracted from the transfer plot is 5×10^{-4} cm^2/Vs with a current $I_{on}/I_{off} \sim 10^4$, with most TFT performance parameters almost independent of growth temperature. In contrast, **DHCO-4TCO**

(25) Sze, S. M. *Physics of Semiconductor Devices*, 2nd ed.; John Wiley & Sons: Taipei, Taiwan, 1981.

(26) (a) Chiechi, R. C.; Sonmez, G.; Wudl, F. *Adv. Funct. Mater.* **2005**, *15*, 427. (b) Donat-Bouillud, A.; Mazerolle, L.; Gagnon, P.; Goldenberg, L.; Petty, M. C.; Leclerc, M. *Chem. Mater.* **1997**, *9*, 2815.

(27) Yoon, M.-H.; Kim, C.; Facchetti, A.; Marks, T. J. *J. Am. Chem. Soc.* **2006**, *128*, 12851.

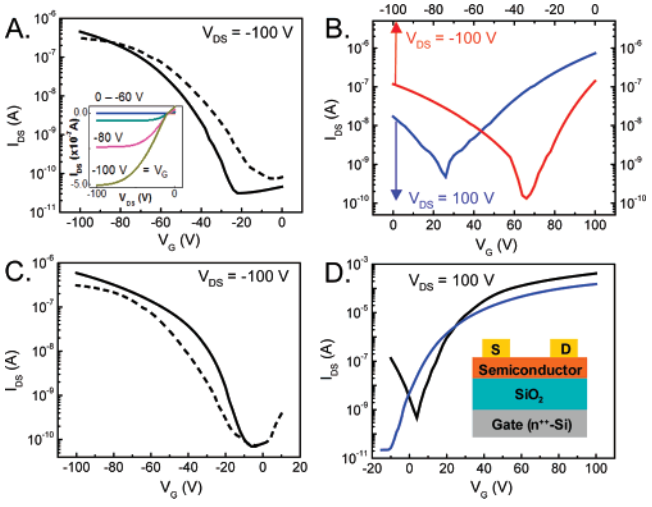

Figure 9. I_{DS}-V plots for (A) **DHCO-4TCOp** (p-type), (B) **DHCO-4TCO** (ambipolar; p-type-red, n-type-blue), (C) **DFHCO-4TCOp** (p-type), and (D) **DFHCO-4T** (n-type-black) and **DFHCO-4TCO** (n-type-blue). The dashed lines represent TFT data using solution-cast films as the semiconductor.

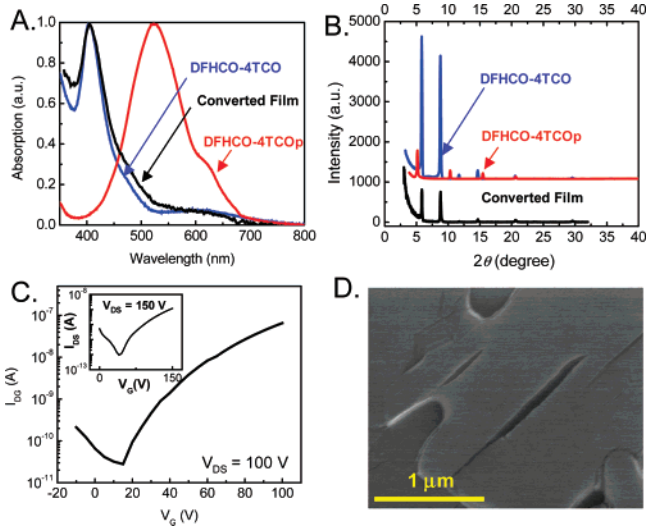

Figure 10. (A) UV−vis spectra and (B) XRD θ−2θ scans showing **DFHCO-4TCOp** to **DFHCO-4TCO** film conversion. (C) Transfer plots of TFTs fabricated by the deprotection conversion of vapor-deposited and solution-cast (inset) films and (D) SEM image of a converted vapor-deposited film.

exhibits ambipolar activity, similar to **DHCO-4T,** with electron and hole mobilities of 0.002 and 2×10^{-4} cm^2/Vs, respectively. Replacing the bulky protecting group in the core by a bridging carbonyl group presumably allows efficient intermolecular packing in the solid-state/film and facilitates transport of both holes and electrons.

Figure 9C,D shows the OTFT response characteristics of the perfluoroacyl-derivatized oligothiophenes **DFHCO-4T**, **DFHCO-4TCOp**, and **DFHCO-4TCO**. Depending on the chemical modification of the conjugated core, either n- or p-type behavior is observed, while the fluorine-free acyl analogues behave as either ambipolar or p-type semiconductors. Insertion of the dioxolane group into the thiophene core inverts the majority charge carrier type from electrons (**DFHCO-4T**) to holes (**DFHCO-4TCOp**) in a very similar fashion to **DHCO-4TCOp**. However, upon introduction of the carbonyl group into the core, the **DFHCO-4TCO** data reveal that n-type activity is recovered with a mobility and on−off ratio 0.08 cm^2/Vs and 10^6, respectively, for films grown at 70 °C. When the deposition temperature is elevated from 25 to 75 °C, the observed n-type mobility and current on−off ratio of **DFHCO-4T** TFT decrease from 0.34 cm^2/Vs and 10^6 to 0.30 cm^2/Vs and 10^5, respectively, and similar effects are also observed in **DFHCO-4TCOp**-based TFTs, opposite to the trend observed in the fluorine-free acyl oligothiophene family.

Finally, top contact thin-film transistors based on solution-cast films of **DHCO-4TCOp** and **DFHCO-4TCOp** were fabricated and tested under vacuum. The **DHCO-4TCOp**/**DFHCO-4TCOp** films were cast on bare SiO_2/p$^+$-Si substrates at temperatures of 110 or 160 °C and concentrations of 0.8 or 0.5 mg/mL, respectively, in 1,2,4-trichlorobenzene solutions. The solvent was slowly evaporated in the saturated solvent-vapor environment, while the substrate was maintained at the aforementioned temperatures for each semiconductor. After annealing overnight in a vacuum oven (100 °C), transistor device fabrication was finalized by depositing gold electrodes for source and drain. The dashed lines in Figure 9A,C represent transfer plots of **DHCO-4TCOp** and **DFHCO-4TCOp**, respectively. Note that **DHCO-4TCOp** solution-cast films exhibit high crystallinity over large areas as demonstrated by film XRD (Figure S5). Remarkably, the saturation-regime mobilities and current on−off ratios of the solution-cast **DHCO-4TCOp** (4×10^{-4} cm^2/Vs, 10^4) and **DFHCO-4TCOp** (2×10^{-4} cm^2/Vs, 10^4) films are very close to those of the vapor-deposited **DHCO-4TCOp** (5×10^{-4} cm^2/Vs, 10^4) and **DFHCO-4TCOp** (3×10^{-4} cm^2/Vs, 10^4) films although the apparent thicknesses (100−200 nm)/microstructural uniformities of the former are greater/poorer than those of the latter. This indicates that semiconductor microstructures favorable for efficient charge transport can be obtained by solution-casting as well as by vapor-deposition, possibly due to the relatively strong/long-range intermolecular interactions in **DHCO-4TCOp** and **DFHCO-4TCOp** films, and that their p-type device performance is relatively insensitive to the film deposition method.

***In Situ* Film Conversion from p-Type to n-Type and Semiconductor Patterning.** Vapor-deposited (50 nm)/solution-cast (100−200 nm) **DFHCO-4TCOp** films on p$^+$-Si/SiO_2 and glass were exposed to saturated H_2O + HCl vapors, while the substrate temperature was maintained at 150 °C. After 1 h, the substrates were placed in a vacuum oven (100 °C) for 3 h to remove absorped gases and ethylene glycol byproduct. After this acidic vapor treatment, the initial purple color of the **DFHCO-4TCOp** film on glass changed to the characteristic green color of **DFHCO-4TCO** film on glass. To examine the possible presence of residual **DFHCO-4TCOp**, even after acid vapor treatment, the film optical spectrum was recorded. Figure 10A shows that the spectrum of the converted film corresponds to that of vapor-deposited **DFHCO-4TCO** with $\lambda_{max} = 405$ nm, while the characteristic 620 nm peak of **DFHCO-4TCOp** disappears. A θ−2θ XRD scan of the treated sample confirms that the film on p$^+$-Si/SiO_2 is converted, showing that the microstructure corresponds to that of **DFHCO-4TCO** (Figure 10B). Note that acidic vapor treatment for an additional 3 h alters neither the UV−vis spectrum nor XRD patterns, indicating that the

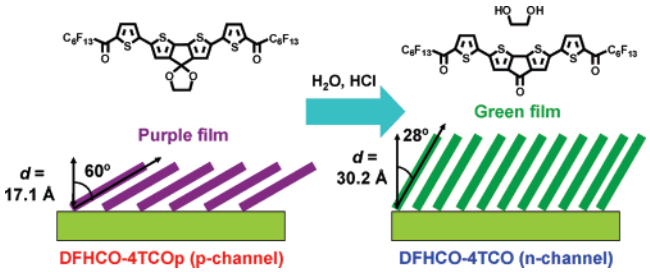

Figure 11. Schematic diagram of *in situ* film conversion from **DFHCO-4TCOp** (left) to **DHCO-4TCO** (right).

in situ film conversion from **DFHCO-4TCOp** to **DFHCO-4TCO** is complete. Volatile HCl and water vapors diffuse into **DFHCO-4TCOp** films, and the dioxolane protecting groups are converted to carbonyl groups in the quaterthiophene core, while ethylene glycol is generated as the byproduct. Interestingly, not only film composition but also the film microstructure, evident in the *d*-spacing, evolves during the conversion process as demonstrated in film XRD scans before and after acid vapor treatment. Considering that the computed molecular lengths of **DFHCO-4TCOp** and **DFHCO-4TCOp** are almost identical (Table 5), the film *d*-spacing increase can be ascribed to changes in molecular packing coincident with the conversion process. As depicted in Figure 11, elevated film temperatures during the conversion process (150 °C) are suggested to facilitate microstructural reorganization to that of vapor-deposited **DFHCO-4TCO** films. After 3 h annealing of the converted films on p^+-Si/SiO_2 at 100 °C under N_2, transistor fabrication is completed by depositing gold source and drain electrodes.

TFTs fabricated after vapor-deposited **DFHCO-4TCOp** film conversion exhibit n-type activity with moderate mobility (2×10^{-4} cm^2/Vs) and current on−off ratio (10^4), while those fabricated from *in situ* converted solution-cast films exhibit poorer n-type mobilities (1×10^{-6} cm^2/Vs) and current on−off ratios (10^3). Pentacene and oligothiophene films have previously been deposited by *in situ* film conversion of a solution-processable precursors;[28,29] however, to our knowledge there have been no reports of *in situ* p-type to n-type film conversion. This approach is particularly intriguing for the complementary circuit fabrication by *in situ* conversion of selectively patterned areas in films thereby creating proximate p- and n-type semiconductor arrays. Finally, note that the relatively modest mobilities and current on−off ratios in TFTs are based on converted films. Although the film composition is altered by the *in situ* conversion process, the SEM images reveal that the film morphology remains essentially intact before and after conversion—as featureless as the parent **DFHCO-4TCOp** films. Since it has been shown that there is a strong correlation between morphology and device performance and that more crystalline morphologies favor efficient electron transport in **DFHCO-4TCO** films, unchanged morphologies even after annealing may partially explain the device performance in the converted films.

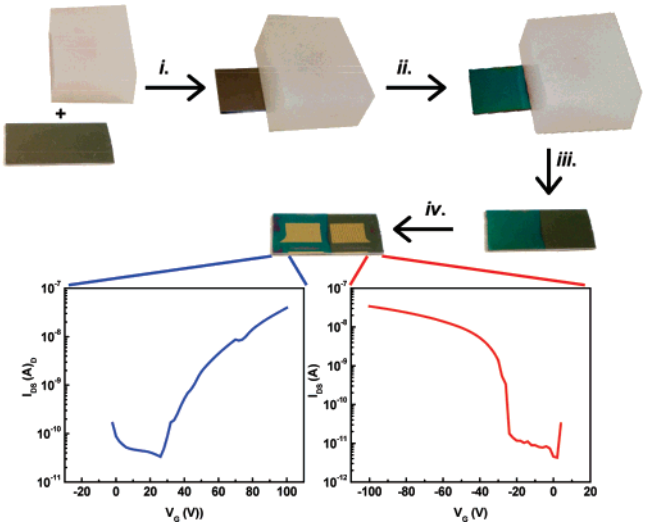

Figure 12. *In situ* conversion-patterning procedure. Top: *i.* fabrication begins by placing a b-PDMS stamp on one-half of a Si−SiO_2-**DFHCO-4TCOp** film substrate; *ii*. exposure to HCl vapor for ∼1 h; and *iii*. removal of the b-PDMS stamp. The unconverted (right) and converted (left) regions are clearly visible. *iv*. Vapor-deposition of Au source/drain contacts. Scratches on the substrates are due to substrate-mask clamping and to access the gate substrate for device testing. Bottom: FET transfer plots showing characteristics n- (left) and p-channel (right) behavior.

To demonstrate that patterning of n- and p-type semiconductor regions on the same substrate is feasible, **DFHCO-4TCOp** films on Si−SiO_2 substrates were subjected to the procedure shown in Figure 12. Briefly, one-half of a **DFHCO-4TCOp** film is protected with a basic-PDMS (b-PDMS) stamp (see the Experimental Section for details), and then the specimen is treated with H_2O−HCl vapor. After removal of the stamp, the protected area (right side) is unchanged, whereas the exposed side exhibits the characteristic green appearance of the **DFHCO-4TCO** films. This is a visual demonstration of the formation of patterned unconverted/converted regions. Furthermore, to demonstrate that the unconverted/converted regions correspond active to p-/n-channel characteristics, FETs were fabricated on either side of the substrate. The devices evaluated on the right side behave as p-channel transistors ($\mu_h = 7 \times 10^{-4}$ cm^2/Vs, $I_{on}/I_{off} = 10^5$, and $V_T = -16$ V) with comparable performance to the unpatterned **DFHCO-4TCOp** films ($\mu_h = 3 \times 10^{-4}$ cm^2/Vs, $I_{on}/I_{off} = 10^4$, and $V_T = -32$ V). This demonstrates that b-PDMS provides conformal film contact, blocking the acidic vapor from contacting the film beneath it, and that it does not compromise the performance of the contacted **DFHCO-4TCOp** film. In contrast, the devices fabricated on the uncovered substrate side behave as n-channel transistors ($\mu_e = 1 \times 10^{-4}$ cm^2/Vs, $I_{on}/I_{off} = 10^4$, and $V_T = 32$ V), and the FET transfer characteristics (while not optimized) are comparable to those of the converted unpatterned **DFHCO-4TCO** films discussed above ($\mu_e = 2 \times 10^{-4}$ cm^2/Vs and $I_{on}/I_{off} = 10^4$). These measurements show that it is possible to pattern the area undergoing *in situ* conversion of a charge carrier type via a nondestructive contact stamp method.

(28) (a) Akinaga, T.; Yasutake, S.; Sasaki, S.; Sakata, O.; Otsuka, H.; Takahara, A. *Chem. Lett.* **2006**, *35*, 1162. (b) Weidkamp, K. P.; Afzali, A.; Tromp, R. M.; Hamers, R. J. *J. Am. Chem. Soc.* **2004**, *126*, 12740.
(29) (a) Murphy, A. R.; Fechet, J. M. J.; Chang, P.; Lee, J.; Subramanian, V. *J. Am. Chem. Soc.* **2004**, *126*, 1596. (b) Chang, P. C; Lee, J.; Huang, D.; Subramanian, V.; Murphy, A. R.; Frechet, J. M. J. *Chem. Mater.* **2004**, *16*, 4783.

Discussion

Chemical Substituent Effects on Majority Carrier Type. Semiconductors **1**−**6** share the same basic quaterthiophene structural motif with carbonyl groups at α,ω skeletal positions of the oligothiophene. Despite such similarities in thiophene backbone structure among semiconductors **1**−**6**, chemical modification in the peripheral (alkyl vs. perfluoroalkyl) and/or core positions (no functionality vs. bridging dioxolane vs bridging carbonyl) of the conjugated oligothiophenes introduces great variation in film microstructural/electrical/semiconducting properties. In both acyl and perfluoroacyl quaterthiophene families, introduction of the dioxolane functionality in the core induces **DHCO-4TCOp** and **DFHCO-4TCOp** to switch to p-type from amibipolar and n-type transport, respectively, while the additional carbonyl group in the conjugated core essentially leaves the semiconductor polarity unchanged versus series members without this core modification. Consequently, **DHCO-4T**/**DHCO-4TCO** and **DFHCO-4T**/**DFHCO-4TCO** exhibit ambipolar and monopolar n-type behavior, respectively, although other performance parameters such as mobility and the on−off ratio vary depending on details of the molecular structures and film growth conditions. Particularly interesting is the p-type behavior of **DHCO-4TCOp** and **DFHCO-4TCOp**, which is in drastic contrast to the trend in other members of the acyl and perfluoracyl oligothiophene families. Note that these dioxolane-derivatized quaterthiophenes are still functionalized with strong electron-withdrawing substituents (acyl or perfluoroacyl) and that these quaterthiophenes are expected to retain planar core geometries and cofacial solid-state packing even after dioxolane attachment, based on the single-crystal structure of **DHCO-4TCOp**.

From the HOMO and LUMO energy level estimations derived from the optical and electrochemical data for quaterthiophene semiconductors **1**−**6**, it is possible to identify correlations between substituent-induced molecular orbital energy modulation, the apparent carrier polarity of the corresponding thin-film transistors (p-, n-type, and ambipolar), and a simple Schottky-type charge injection barrier model for carrier polarity.[30,7a] This qualitative model was previously successful in explaining majority carrier type trends in several homologous series of alkyl/fluoroalkyl-substituted oligothiophenes. In this model, relative hole and electron injection rates have an exponential dependence on the injection barrier (ΔE_e or ΔE_h), assumed to be the difference between the metal electrode Fermi level and the HOMO/LUMO energy levels for hole/electron transport. Estimated HOMO/LUMO energy levels and band gap energies of **DH-4T**, **DFH-4T**, and semiconductors **1**−**6** including the Fermi level of the gold electrode (∼5 eV)[31] are depicted in Figure 13.

From the aforementioned Schottky injection barrier model, an increase in the reduction potential resulting from acyl group functionalization should lower the electron injection barrier and possibly facilitate n-type behavior, all other factors being approximately equal (Marcus reorganization energies, intermolecular orbital overlap, interface dipoles, charge traps, etc.). As discussed in the previous section, both **DHCO-4T** and **DHCO-4TCO** exhibit efficient electron-transport properties with electron mobilities as high as 0.12 cm^2/Vs in addition to hole-transporting properties, while **DH-4T** exhibits only p-type behavior. Such ambipolar behavior in **DHCO-4T** and **DHCO-4TCO** can be explained by approximately balanced hole- and electron-injection barrier heights (with respect to the gold Fermi level), while the former is much lower than the latter in p-type-only **DH-4T** and **DHCO-4TCOp**. The p-type-only activity exhibited by **DHCO-4TCOp** can be understood from the standpoint of the relatively high HOMO level, which substantially lowers the hole injection barrier and enhances p-type activity vs. n-type. Note that the effective conjugation and the resultant decreased band gap energy due to the α,ω-carbonyl functionalization contributes to raising the HOMO level in **DHCO-4TCOp**. In the case of perfluoroacyl oligothiophenes, LUMO energy levels are further depressed by the combined electron-withdrawing power of the acyl and perfluoroalkyl groups, with **DFHCO-4T** and **DFHCO-4TCO** exhibiting monopolar electron transport rather than ambipolar behavior.

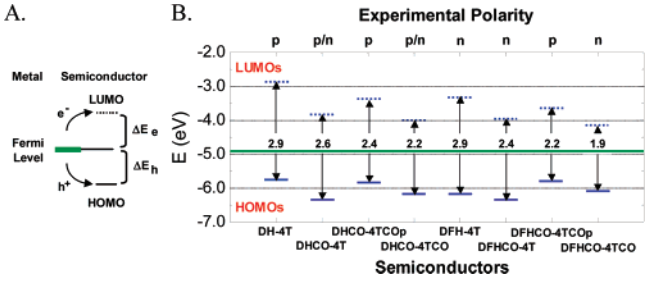

Figure 13. (A) Schematic of a simple Schottky-type barrier between a metal electrode and a contacting semiconductor. ΔE_e and ΔE_h represent electron and hole injection barriers, respectively. (B) HOMO and LUMO energy diagrams for **DH-4T**, **DFH-4T**, and semiconductors **1**−**6**. Experimental polarity of semiconductors depicted in the top axis. The green line corresponds to Fermi level of a gold electrode (4.9 eV).

Growth Temperature Effects on Film Morphology and Transistor Response. Among both the acyl and perfluoroacyl quaterthiophene families, strong correlations between film morphological features and semiconductor performance parameters are observed when the semiconductor and film growth temperature are varied. In the acyl quaterthiophene series, **DHCO-4T** and **DHCO-4TCO** films grown on 70 °C substrates exhibit larger grains/vertical walls than those deposited on 25 °C substrates. Note that such morphological features in films grown at higher substrate temperatures correlate with more favorable semiconductor performance parameters such as higher mobilities and higher current on−off ratios (Table 6). In contrast to the **DHCO-4T** and **DHCO-4TCO** films, **DHCO-4TCOp** films exhibit completely featureless morphologies, and such morphological characteristics are closely related to the observed TFT performance parameters of the corresponding semiconductors. While **DHCO-4T** and **DHCO-4TCO** films exhibit relatively large mobilities, **DHCO-4TCOp** films exhibit

(30) (a) Mahapatro, A. K.; Ghosh, S. *Appl. Phys. Soc.* **2002**, *80*, 4840. (b) Chwang, A. B.; Frisbie, C. D. *J. Phys. Chem. B* **2000**, *104*, 12202.
(31) Hill, I. G.; Rajagopal, A.; Kahn, A. *J. Appl. Phys.* **1998**, *84*, 3236.

Table 6. Majority Charge Carrier Types, TFT Mobilities (μ), Threshold Voltages (V_T), and Current On−Off Ratios (I_{on}/I_{off}) as a Function of Deposition Temperature (°C) for Vapor-Deposited (50 nm) and Solution-Cast Films (100−200 nm, in Parentheses) of DH-4T, DFH-4T, and Semiconductors 1−6 on HMDS-Treated Si/p$^+$-SiO$_2$ Substrates[a]

		μ (cm^2/Vs)		V_T (V)		I_{on}/I_{off}	
semiconductors		70 °C	25 °C	70 °C	25 °C	70 °C	25 °C
DH-4T[b]	p	0.04	0.06	−3	−10	10^6	10^6
	n	0.12	0.013	35	30	10^7	10^4
DHCO-4T	p	0.008	2×10^{-4}	−54	−40	10^7	10^3
DHCO-4TCOp	p	5×10^{-4} (4×10^{-4})	5×10^{-4}	−35 (−33)	−40	10^4 (10^4)	10^4
	n	0.002	2×10^{-5}	57	72	10^3	10^3
DHCO-4TCO	p	2×10^{-4}	6×10^{-6}	−54	−36	10^3	10^3
DFH-4T[b]	n	0.06	4×10^{-4}	27	40	10^5	10^3
DFHCO-4T	n	0.32	0.34	38	32	10^5	10^6
DFHCO-4TCOp	p	3×10^{-4} (2×10^{-4})	6×10^{-4}	−32 (−39)	−30	10^4 (10^4)	10^5
DFHCO-4TCO	n	0.08	0.005	9	43	10^7	10^6

[a] SiO$_2$ dielectric (300 nm, $C_i = 10$ nF/cm^2); $L = 100$ μm, $W = 5$ mm. Measured in a vacuum probe station. [b] From ref 7a.

relatively poor mobilities and current on−off ratios in OTFT devices. In previous studies of regiochemically varied perfluroarene-thiophene oligomers,[8] a similar correlation of morphology and OTFT performance was observed, suggesting that highly interconnected crystalline textures are more favorable for charge transport in the organic semiconducting films than almost featureless smooth morphologies.

In contrast, **DFHCO-4T** and **DFHCO-4TCOp** films grown at 25 °C exhibit more crystalline morphologies with larger grains than those grown at 70 °C, which is opposite to the trend observed in the acyl oligothiophene family. In the case of **DFHCO-4T**, these growth temperature effects on film morphology are more pronounced (Figure 8C), and the poor crystallinity and featureless morphologies of the films grown at 70 °C corresponds to inferior transistor performance parameters such as lower mobility and current on−off ratio. Recalling that the XRD scans of **DFHCO-4T** films deposited at 25 and 70 °C reveal highly crystalline microstructures and identical Bragg progressions with a single dominant phase, the poorer device characteristics for 70 °C deposition, especially the low current on−off ratios, can be related to morphological features such as long cracks and lack of crystalline interconnectivity. Such discontinuities may generate greater trap densities and unintended doping, thereby including V_T shifts to more positive voltages and reduction of current on−off ratios. Such inverse proportionality between deposition temperature and device performance parameters and sharply peaked optimum deposition temperatures was previously observed in several perfluoroalkyl-derivatized oligothiophenes and phenylene-thiophene oligomers.[7,32]

Conclusions

The present contribution describes a full account of the syntheses and molecular/thin-film properties of two new families of acyl and perfluoroacyl quaterthiophenes and their device fabrication/characterization. Insertion of carbonyl functionality into the oligothiophene skeleton induces sizable alterations in molecular orbital energies and crystal packing compared to the carbonyl-free parent derivatives. Optical and electrochemical molecular characterization data demonstrate that terminal/central carbonyl-functionalization of the quaterthiophene core reduces both HOMO and LUMO energies. However, the extent of LUMO energy depression is much larger than the HOMO energy variation, with the outcome being that carbonyl-containing quaterthiophenes exhibit lower energy gaps vs. the corresponding parent systems. This greater LUMO stabilization is confirmed by electrochemical data and fully explained by DFT computations of the electronic structure. The HOMOs of **1**−**6** exhibit poor conjugation between the thiophene central portion and the carbonyl fragments because of the presence of nodal planes, whereas the LUMOs fully extend to the carbonyl groups. Furthermore, thermal and single-crystal structural characterization demonstrate that C═O insertion enhances mesophase formation and strongly alters molecular packing characteristics from herringbone-like for alkyl/fluoroalkyl-substituted and unsubstituted quaterthiophenes to slipped cofacial for **DFPCO-2T** and compound **2**.

OFET performance demonstrates that device parameters such as carrier polarity, carrier mobility, and current on−off ratio are also greatly modified by carbonyl-incorporation. Very large n-type (up to 0.32 cm^2/Vs), p-type (up to 0.04 cm^2/Vs), and ambipolar (up to 0.12 cm^2/Vs for electrons and 0.008 cm^2/Vs for holes) mobilites are observed in transistors based on this class of materials. We have explained the carrier polarity trends in terms of a simple Schottky injection barrier model where the electrochemically derived HOMO and LUMO energy levels are balanced evenly with respect to the Fermi level of the Au electrode, thereby facilitating injection of either holes or electrons based on the applied bias polarity. In addition, we have correlated the large mobilites of **DHCO-4T** and **DFHCO-4T** with favorable film texturing and morphology trends evident in SEM and film XRD characterizations. Although the HOMO levels of **DHCO-4TCOp** and **DFHCO-4TCOp** align favorably with the gold electrode Fermi level for hole injection, the modest hole mobilities for these systems (5×10^{-4} cm^2/Vs and 4×10^{-4} cm^2/Vs, respectively) observed for both vapor- and solution-grown films are consistent with the unfavorable molecular packing observed in the crystal structure of **2**. Clearly an interplay of frontier molecular orbital energies, molecular packing, and thin-film microstructure and morphology (molecular packing and crystal formation) as well as film processing conditions greatly affect trapping site density at the semiconductor-dielectric interface and govern

(32) Facchetti, A.; Letizia, J.; Yoon, M.-H.; Mushrush, M.; Katz, H. E.; Marks, T. J. *Chem. Mater.* **2004**, *16*, 4715.

charge transport efficiency. Finally, due to the good solubility of the dioxolane-protected derivatives **2** and **5**, the first example of *in situ* conversion of vapor-deposited and solution-cast films from p-type to n-type is demonstrated. Thus **DFHCO-4TCOp (2)** films are converted *in situ* with $HCl-H_2O$ vapor to **DFHCO-4T (3)**, the latter exhibiting an electron mobility of 2×10^{-4} cm^2/Vs. Furthermore, a proof-of-concept PDMS contact patterning methodology creates p- and n-channel regions on the same substrate and provides a new approach to organic CMOS device fabrication.

Acknowledgment. We thank ONR (N00014-02-0909), the NSF-MRSEC program through the Northwestern Materials Research Center (DMR-0076097), and the NASA Institute for Nanoelectronics and Computing (NCC 2-3163) for support of this research.

Supporting Information Available: Single-crystal X-ray determination data, optical PL spectra, DSC/TGA analysis, XRD scans, and computed structures (Table S1 and Figures S1−S4). This material is available free of charge via the Internet at http://pubs.acs.org.

CM071230G